Chemical Geology xxx (xxxx) 121979

Contents lists available at ScienceDirect

Chemical Geology

journal homepage: www.elsevier.com/locate/chemgeo

Extensive H_2O degassing in deeply erupted submarine glasses inferred from Samoan melt inclusions: The EM2 mantle source is damp, not dry

Olivia E. Anderson [a,*], Matthew G. Jackson [a], Ayla S. Pamukçu [b,c], Estelle F. Rose-Koga [d], Véronique Le Roux [b], Frieder Klein [b], Kenneth T. Koga [d], Glenn A. Gaetani [b], Allison A. Price [a]

[a] Isotope Geochemistry Facility – Global Center for Mantle Zoology (GCMZ), University of California Santa Barbara, Department of Earth Science, Santa Barbara, CA, USA
[b] Woods Hole Oceanographic Institution, Woods Hole, MA 02543, USA
[c] Geological Sciences, Stanford University, Stanford, CA, USA
[d] Institut des Sciences de la Terre d'Orléans (ISTO), UO/CNRS/BRGM, 1A rue de la Férollerie, 45071 Orléans, France

ARTICLE INFO

Editor: Dr. S Aulbach

Keywords:
Melt inclusion
Samoa
Hotspot
Degassing
Enriched mantle
H_2O

ABSTRACT

Submarine glasses erupted at intraplate volcanic hotspot settings sampling enriched mantle (EM)—characterized by high $^{87}Sr/^{86}Sr$—exhibit lower H_2O/Ce than glasses representing less enriched mantle domains, leading to the interpretation that the EM mantle is H_2O-poor ("dry"). We test whether low H_2O/Ce observed in pillow glasses of EM lavas resulted from degassing of higher H_2O/Ce primary melts by measuring H_2O/Ce and $^{87}Sr/^{86}Sr$ in olivine-hosted melt inclusions from two deeply-erupted (3950 and 2190 m below sea level (mbsl)) Samoan submarine lavas from Vailulu'u and Malumalu seamounts. Vailulu'u (H_2O/Ce = 161–275) and Malumalu (149–232) melt inclusions have an average H_2O/Ce (197 ± 58 2SD, N = 15) that is nearly twice as high as H_2O/Ce in pillow glasses from these two seamounts (average H_2O/Ce = 106 ± 51, N = 65), and comparable to pillow glasses from non-EM hotspots. We show that lower H_2O/Ce in submarine Samoan glasses compared to melt inclusions results from greater closed-system degassing, and concomitant loss of H_2O, because EM melts have higher initial concentrations of CO_2. We show that the lower H_2O/Ce in global EM pillow glasses compared to non-EM pillow glasses can be modeled to be the result of more extensive degassing of H_2O in EM melts, which owes to higher CO_2 in primary melts (20,000–90,000 ppm) of EM sources compared to non-EM melts (300–50,000 ppm CO_2). Instead of originating from a dry mantle, we conclude that EM lavas derive from a damp mantle, but EM melts lose more H_2O by degassing than non-EM melts.

1. Introduction

Although volatiles are a minor component in silicate melts, they play an outsize role on the properties and behavior of magmatic systems. Hydrogen and carbon affect the depth and extent of melting, the composition of melts, how melts evolve, and also the rheology of the mantle (e.g., Asimow and Langmuir, 2003; Gaetani and Grove, 1998; Hirschmann, 2006; Hirth and Kohlstedt, 1996; Hirth and Kohlstedf, 2003; Portnyagin et al., 2007). Therefore, connecting volatile element compositions to mantle domains characterized by particular isotopic compositions, such as enriched mantle (EM), can provide additional insights into mantle heterogeneities. A variety of geochemical "flavors" have been identified in the mantle via geochemical taxonomy of ocean island basalts (OIB) (e.g., Hart et al., 1986; Hart, 1988; Hofmann and White, 1982; Zindler and Hart, 1986), and the various mantle species are broadly encompassed by several canonical mantle endmembers that include HIMU (high $\mu = {}^{238}U/{}^{204}Pb$), EM1 (enriched mantle 1), EM2 (enriched mantle 2), and DM (depleted mantle). Samoan lavas have unique geochemical signatures that extend to Enriched Mantle 2 (EM2) isotopic compositions (e.g., high $^{87}Sr/^{86}Sr$, intermediate $^{206}Pb/^{204}Pb$, and low $^{143}Nd/^{144}Nd$). The EM2 mantle source has been suggested to be derived from recycled continental materials (e.g., White and Hofmann, 1982; White and Duncan, 1996; Jackson and Macdonald, 2022). Therefore, characterization of Samoan EM2 lavas can provide insights into the role that deep continental crust subduction plays in controlling the volatile budgets of the mantle.

The ratios H_2O/La or H_2O/Ce measured in submarine glasses are commonly used to evaluate H_2O enrichment or depletion in the mantle because H_2O, La, and Ce have similar degrees of incompatibility (e.g., Michael, 1995). Thus, their ratios are not significantly affected by partial melting and crystal fractionation. The EM2 mantle source has been interpreted to be 'dry' because the H_2O/Ce (or H_2O/La) is lower at

* Corresponding author.
E-mail address: anderson03@ucsb.edu (O.E. Anderson).

https://doi.org/10.1016/j.chemgeo.2024.121979
Received 30 October 2023; Received in revised form 31 January 2024; Accepted 2 February 2024
0009-2541/© 20XX

UNCORRECTED PROOF

Note: Low-resolution images were used to create this PDF. The original images will be used in the final composition.

higher $^{87}Sr/^{86}Sr$ for Samoan glasses (Workman et al., 2006). Workman et al. (2006) found that H_2O/La anticorrelates with $^{87}Sr/^{86}Sr$: the more geochemically enriched (higher $^{87}Sr/^{86}Sr$) Samoan glasses have lower H_2O/La than more geochemically depleted Samoan glasses; the high H_2O/La MORB mantle endmember anchors the low $^{87}Sr/^{86}Sr$ portion of the array. Workman et al. (2006) explained this relationship between $^{87}Sr/^{86}Sr$ and H_2O/La as the result of diffusive H_2O loss from EM2 reservoirs during long-term storage in a dry and depleted mantle, resulting in a "dry" EM2 mantle domain that has low H_2O/La and low H_2O. Similarly, Dixon et al. (2002) found that high $^{87}Sr/^{86}Sr$ basalts erupted in MOR settings had low H_2O/Ce. However, unlike Workman et al. (2006), Dixon et al. (2002) suggested that the dry nature of the EM reservoir was due to dehydration of sediments during subduction, resulting in low H_2O/Ce signatures in subducted, dehydrated sediments, which ultimately contribute to enriched mantle domains. Bizimis and Peslier (2015) offered further discussion regarding the origin of apparently dry EM2 domains and argued that the low H_2O/Ce in EM lavas is the result of recycling of pyroxenite-bearing oceanic lithosphere. The pyroxenites they examined have low H_2O/Ce and high H_2O, a result of preferential partitioning of Ce into clinopyroxene compared to H_2O.

Additional work highlights the low H_2O/Ce in enriched mantle domains (Kendrick et al., 2017). In particular, classical EM1 and EM2 oceanic hotspots—Pitcairn and Societies, respectively—exhibit negative correlations between $^{87}Sr/^{86}Sr$ and H_2O/Ce in submarine glasses (Kendrick et al., 2014). Thus, low H_2O/Ce appears to be a defining feature of EM lavas, and constraining the origin of this geochemical signature is critical for understanding the origin of the EM mantle and/or the petrogenesis of EM lavas.

Existing models for the origin of low H_2O/La and H_2O/Ce in EM-flavored OIB pillow glasses quenched in deep submarine environments are predicated on the assumption that the low H_2O/Ce is a source feature and the EM primary melts have low H_2O/Ce inherited from the mantle source (Dixon et al., 2002; Dixon and Clague, 2001; Wallace, 2002; Workman et al., 2006; Kendrick et al., 2014). This interpretation assumes that magmatic degassing follows open system behavior, a mechanism that results in significant loss of CO_2, but not H_2O, from the melt by degassing: the H_2O/Ce in deeply erupted glasses (i.e., ≥0.1 kbar; Workman et al., 2006) resulting from this process are similar to the mantle source despite having degassed most of their magmatic CO_2.

In this study, we test this assumption using combined H_2O/Ce and $^{87}Sr/^{86}Sr$ measurements in individual olivine-hosted melt inclusions isolated from two well-characterized submarine Samoan basalts that were characterized by Workman et al. (2006). We present volatile (H_2O, CO_2, Cl, F, S), major, and trace element concentrations and $^{87}Sr/^{86}Sr$ on Samoan melt inclusions from both samples—AVON3-78-1 and AVON3-71-2—which were obtained from Malumalu and Vailulu'u seamounts, respectively. Malumalu lavas reach $^{87}Sr/^{86}Sr$ of up to 0.708901, which is the most extreme EM2 composition that we explore in this study. In contrast, Vailulu'u lavas have $^{87}Sr/^{86}Sr$ that range from 0.705352 to 0.706720, and thus represent a less enriched composition at the Samoan hotspot. Previous $^{87}Sr/^{86}Sr$ analyses of Samoan melt inclusions demonstrated extreme heterogeneity (0.70434 to 0.70926) that has been verified using both in situ LA-ICP-MS approach (laser-ablation inductively coupled plasma mass spectrometry; Jackson and Hart, 2006) and an approach involving wet chemistry followed by TIMS (thermal ionization mass spectrometry; Reinhard et al., 2018). Critically for this study, the melt inclusions from the two lavas examined here span nearly the same range of $^{87}Sr/^{86}Sr$ (0.704858–0.709225) as identified in prior melt inclusion studies (Jackson and Hart, 2006; Reinhard et al., 2018) and have similar trace element characteristics as the Samoan pillow glasses examined for H_2O/La and $^{87}Sr/^{86}Sr$ by Workman et al. (2006) (0.704521–0.708901). We interpret this to indicate that the melt inclusions thus sample the same mantle sources as the pillow glasses studied by Workman et al. (2006).

However, Samoan melt inclusions in this study exhibit two key differences with the Samoan submarine glasses reported in Workman et al. (2006): 1) the melt inclusions have higher H_2O/Ce than Samoan submarine glasses and 2) the inclusions exhibit no relationship between H_2O/Ce and $^{87}Sr/^{86}Sr$, which contrasts with the negative correlation between $^{87}Sr/^{86}Sr$ and H_2O/Ce observed in Samoan pillow glasses. We model the difference in H_2O/Ce between melt inclusions and pillow glasses as being a result of closed-system degassing, a mechanism that results in greatly diminished CO_2 *and* H_2O concentrations in the melt (in contrast to open-system degassing, which results in greatly diminished CO_2, but not H_2O, melt concentrations). During closed-system degassing, also called equilibrium or batch equilibrium degassing (e.g., Gerlach and Taylor, 1990), the CO_2 is exsolved as a gas phase, but remains in isotopic equilibrium with the melt. In open-system degassing, also called fractional equilibrium degassing or Rayleigh distillation, an infinitesimally small quantity of the equilibrium gas phase is exsolved and escapes from the melt, thus changing the composition of the system. This results in the isotopic composition of the total sum of the gas phase being out of equilibrium with the melt, and the CO_2 is stripped off from the melt more efficiently than in closed-system degassing. In our closed-system degassing model, the melt inclusions experience less closed-system degassing compared to submarine glasses because of deep entrapment of the melt inclusions in growing olivine crystals within magma chambers. Melts that were not trapped continued to degas both CO_2 and H_2O up until eruption and quenching on the seafloor, resulting in lower H_2O/Ce in the submarine glasses compared to the deeply entrapped melt inclusions.

We also present a model suggesting that, across global oceanic hotspots, primary melts with higher $^{87}Sr/^{86}Sr$ (e.g., Samoan and Societies EM2 glasses, Pitcairn EM1 glasses) have higher primary melt CO_2 than lower $^{87}Sr/^{86}Sr$ melts (e.g., Foundation, Hawai'i (Lō'ihi), and Easter hotspots). Higher CO_2 in high $^{87}Sr/^{86}Sr$ (EM) melts results in greater degassing of both CO_2 and H_2O (and a greater reduction in the H_2O/Ce ratio) compared to low $^{87}Sr/^{86}Sr$ melts, which explains the negative global correlation between H_2O/Ce and $^{87}Sr/^{86}Sr$ in OIB glasses. This new result suggests that submarine glasses sourcing EM domains do not provide reliable records for evaluating the H_2O and H_2O/Ce in the mantle source. In melt inclusions, degassing is arrested at great depth, making it possible to identify H_2O/Ce ratios that are closer to values in the primary melt.

2. Methods

Submarine pillow basalt samples in this study are from two Samoan seamounts (Fig. 1) that are young (< 8 ka; Sims et al., 2008) and associated with visually fresh lavas: Malumalu (sample AVON3-78-1; 2260–2190 mbsl) and Vailulu'u (sample AVON3-71-2; 4420–3950 mbsl) are olivine-rich lavas with glassy chill margins on the pillow rims. Olivine-hosted melt inclusions from Vailulu'u and Malumalu seamounts in this study were rehomogenized on a heating stage (see supplement for methods), and these rehomogenized inclusions were then characterized for $^{87}Sr/^{86}Sr$ (15 melt inclusions total), $^{143}Nd/^{144}Nd$ (only three melt inclusions), stable hydrogen isotope ratios (δD), and major, trace and volatile element concentrations (Table S1). This supplement also includes methodological details for the glass major element (electron probe microanalyzer (EPMA)), volatile (H_2O, CO_2, F, Cl, S) (secondary ion mass spectrometry (SIMS)), hydrogen isotope (SIMS), and trace element (LA-ICP-MS) analyses and the host olivine major element (EPMA) analyses. Strontium separation chemistry and $^{87}Sr/^{86}Sr$ analyses by TIMS used in this study follow the same procedure as described in Anderson et al. (2021). The supplement includes details of Nd separation chemistry for melt inclusions, and $^{143}Nd/^{144}Nd$ analyses by TIMS at the University of California, Santa Barbara Isotope Geochemistry Facility. Only three melt inclusions (all from the Vailulu'u Seamount sample) in this study had sufficient Nd for the isotopic analysis.

CORRECTED PROOF

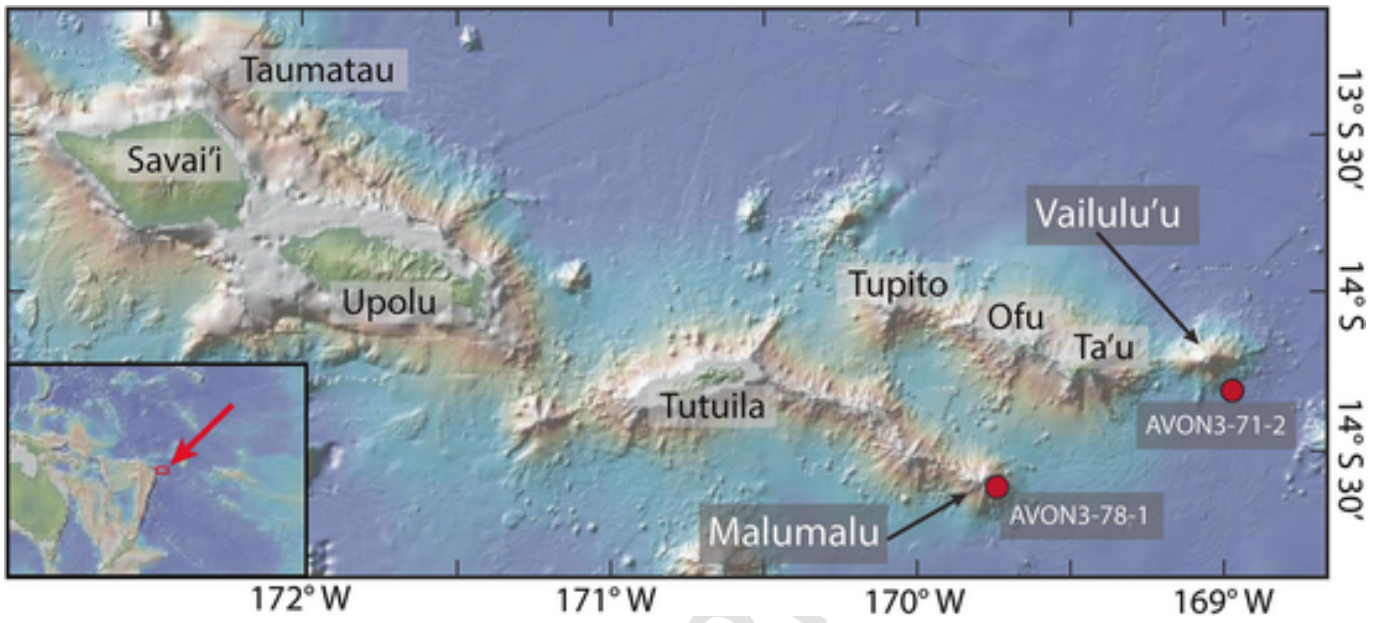

Fig. 1. Map of the Samoan Islands. Red dots indicate the location of AVON3 cruise dredge sites 71 and 78, from the flanks of Vailulu'u and Malumalu, respectively. Map created using GeoMapApp (www.geomapapp.org; Ryan et al., 2009). (For interpretation of the references to color in this figure legend, the reader is referred to the web version of this article.)

The results of in situ analyses (of δD, and major, trace and volatile element concentrations) of geologic reference materials (ALV519-4-1, ALV1833-1, GL07 D52-5, and BCR-2) and values from the literature for these geologic reference materials can be found in Table S2, and $^{87}Sr/^{86}Sr$ and $^{143}Nd/^{144}Nd$ analyses of BCR-2 can be found in Tables S6 and S8. Our measurement of H_2O concentrations in ALV519-4-1 and ALV1833-1 are 1.6% and 1.2%, respectively, different from our preferred values for H_2O in ALV519-4-1 (Bryan and Moore, 1977) and ALV1833-1 (Kumamoto et al., 2017). Our measurement of Ce in ALV519-4-1 differs from Gale et al. (2013) by ~3.4%.

Melt inclusion major, trace, and volatile element concentrations were corrected for post-entrapment crystallization (PEC) by addition or subtraction of equilibrium olivine in 0.1% increments until the major element composition of the inclusion is in equilibrium with the host olivine forsterite (Fo) content (e.g., Danyushevsky et al., 2000). In the calculation, two assumptions are made: (i) the olivine-melt Fe—Mg K_d = 0.30 (Roeder and Emslie, 1970; Ford et al., 1983; $K_d = (Fe^{2+}/Mg)_{olivine}/(Fe^{2+}/Mg)_{melt}$) and (ii) Fe^{3+} comprises 10% of the total moles of iron in the melt (following Hauri, 1996). Unless stated otherwise, all major, trace, and volatile element concentrations reported below have been corrected for equilibrium olivine addition/subtraction so that the inclusion is in equilibrium with the host olivine.

The supplement also details the method of accounting for all CO_2 within a melt inclusion, including both the CO_2 in the glass analyzed by SIMS, the CO_2 contained within the vapor bubble obtained by Raman spectroscopy, and the volumes of bubble and glass for each melt inclusion obtained by X-ray computed microtomography (see Table S3 for the method of reconstructing the total CO_2 content of each melt inclusion and supplementary section S1.3 for analytical methods).

3. Methods for data treatment

We use a series of criteria to identify inclusions where the volatile contents have been compromised. This way the results and discussion can focus on primary magmatic signatures. Fig. 2 shows all melt inclusions from which we collected volatile data. Inclusions whose volatile contents were likely compromised are designated with a black "x" in Fig. 2. We do not consider these inclusions further in our data analysis and interpretation so as to focus on primary magmatic signatures.

Inclusions are excluded if they show evidence of being affected by one or more of the following:

i) *Diffusive proton loss.* Hydrogen isotopes can indicate whether H_2O loss from the melt inclusion has occurred by proton diffusion through the host olivine. Melt inclusions that have been affected by proton diffusion will have low H_2O contents and high δD values due to faster diffusion of hydrogen over deuterium (Hauri, 2002; Gaetani et al., 2012; Bucholz et al., 2013; Hartley et al., 2015). Therefore, we measured δD on all melt inclusions reported in this study. Melt inclusions in the Malumalu sample (AVON3-78-1) have a δD range of −51.8‰ to +127.6‰, and melt inclusions in the Vailulu'u sample (AVON3-71-2) have a δD range of −52.4‰ to −22.0‰ (Fig. 2). Diffusive H_2O loss from melt inclusions should produce a systematic relationship between melt inclusion δD and volume. Melt inclusions from both lavas with volumes $>10^5$ μm³ exhibit no systematic relationship between δD and melt inclusion volume, and they exhibit a relatively narrow range in δD of −35.9 ± 17.4‰ (2SD, N = 18). However, the two melt inclusions with positive δD values, both from Malumalu (samples AVON3-78-1#13 and AVON3-78-1#32), have the smallest volumes (~8.8×10^4 μm³ and 4.3×10^4 μm³). Prior work has shown that smaller volume melt inclusions are more susceptible to diffusive proton loss that results in elevated δD (Hauri, 2002; Gaetani et al., 2012; Bucholz et al., 2013; Hartley et al., 2015). Therefore, the two small-volume inclusions are excluded.

ii) *Breaching.* Two melt inclusions have likely suffered breaching because CO_2 is <200 ppm and H_2O is <1 wt% (see Fig. S4; AVON3-78-1#25, AVON3-78-1#37). Both melt inclusions exhibit melt-filled cracks that intersect the melt inclusions, which is strong physical evidence that supports the breaching interpretation.

iii) *Extremely large vapor bubbles.* Three melt inclusions (AVON3-78-1#10, AVON3-78-1#28, AVON3-71-2#20) have vapor bubbles that make up >10 vol% of the melt inclusion and are excluded. Prior work suggested that large vapor bubbles result from simultaneous entrapment of a mix of melt and CO_2 fluid (e.g.

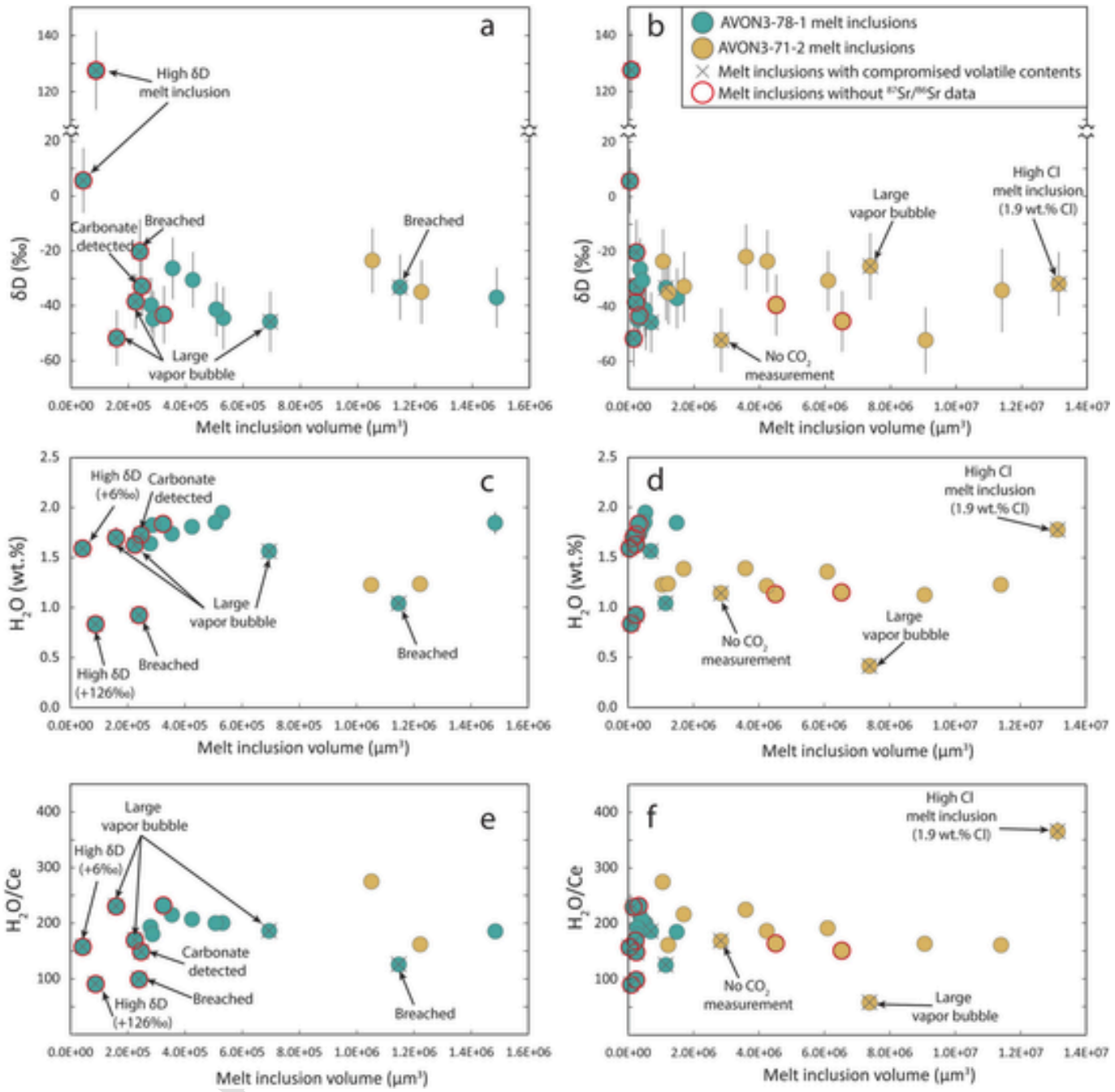

Fig. 2. (a–b) δD (‰), **(c–d)** H_2O (wt%), and **(e–f)** H_2O/Ce versus melt inclusion volume (μm³). Left-hand side panels focus (zoom in) on the Malumalu melt inclusions and right-hand side panels (zoom out) to show the Vailulu'u melt inclusions. In panel (a) δD errors represent the 2σ in run measurement precision of each analysis, which is generally slightly lower than the reproducibility of the secondary standard ALV1833-1 (i.e., ±16‰, 2SD; see Table S2). Melt inclusion H_2O compositions are corrected for olivine addition/subtraction to be in equilibrium with the host olivine (olivine correction is as in Section 2 of the main text). Measurement errors for H_2O, and reproducibility of H_2O analyses on ALV1833-1, are smaller than the data symbol (see Table S2 and Supplementary section S1.6). As discussed in Section 3 of the text, we infer that the volatile contents of eleven melt inclusions shown in this figure have been compromised in one of several ways—hydrogen diffusion loss (and resultant elevated δD), breaching, large vapor bubbles, extremely high Cl concentrations, presence of carbonate, and/or missing Raman-based CO_2 data—and are marked with an "x" symbol. The compromised melt inclusions are not shown in subsequent figures.

Anderson, 1974; Frezzotti, 2001; Hanyu et al., 2020; Moore et al., 2015), which is not representative of melt-only compositions.

iv) *No CO_2 detected by Raman.* No Fermi doublets were observed by Raman spectroscopy for two melt inclusions (AVON3-71-2#14, AVON3-71-2#18), thus the CO_2 densities may have been too low for detection. To err on the side of caution, we are excluding these two melt inclusions from the interpretations of this study. The sample AVON3-71-2#18 that is being excluded for this sole reason (i.e., undetectable CO_2 in the vapor bubble) would not affect the interpretations of this study if it were included. For other excluded melt inclusions, CO_2 densities in the vapor bubbles were highly uncertain (AVON3-71-2#20; ±0.092) or so low that negative values resulted from the calibration (AVON3-78-1#25, AVON3-78-1#37, AVON3-71-2#14), and the volatile data for these four melt inclusions are excluded from the discussion.

v) *Carbonate detected by Raman*. If carbon exists as carbonate in a melt inclusion, the CO_2 budget of the melt inclusion may be underestimated. In this study, carbonates were detected by Raman in two Malumalu melt inclusions (AVON3-78-1#15 and AVON3-78-1#32), and volatile data for these inclusions are excluded.

4. Results

4.1. Hydrogen and strontium isotopes

After filtering the data for the compromised melt inclusions, the Samoan melt inclusions from Malumalu (−38.5 ± 13.5‰, N = 8) and Vailulu'u (−33.9 ± 19.7‰, N = 10) are relatively homogenous in δD with an average δD value of −35.9‰ (±17.4‰, 2SD, N = 18). The Samoan inclusions have heavier δD than most MORB and Lō'ihi (now known as Kama'ehuakanaloa) values, consistent with heavy δD values (ca. -40‰) found in OIBs with recycled components (Loewen et al., 2019).

Critically, $^{87}Sr/^{86}Sr$ measurements in melt inclusions provide a test for whether the Samoan melt inclusions of this study represent the Samoan mantle sources sampled by Vailulu'u and Malumalu glasses. If they do represent the same sources, then the volatile and trace element concentrations of the melt inclusions can be directly compared to concentration measurements in Samoan pillow lava glasses. The $^{87}Sr/^{86}Sr$ range for all of the Malumalu (sample AVON3-78-1) melt inclusions reported here is large, from 0.706594 to 0.709225 (Figs. 3, 4). The inclusions largely fall within the range reported for Malumalu pillow glasses and whole rocks (0.706374–0.708901; Workman et al., 2006). The $^{87}Sr/^{86}Sr$ range for all of the Vailulu'u (sample AVON3-71-2) melt inclusions reported here is smaller compared to AVON3-78-1 melt inclusions, from 0.704858 to 0.705718. The range of Vailulu'u melt inclusion $^{87}Sr/^{86}Sr$ overlaps with the range reported for Vailulu'u pillow glasses (0.705352–0.706720; Workman et al., 2006) but, relative to Vailulu'u pillow glasses and whole rocks, the Vailulu'u melt inclusions are shifted to less radiogenic (lower) $^{87}Sr/^{86}Sr$ values. Taken together, the $^{87}Sr/^{86}Sr$ for the Malumalu and Vailulu'u melt inclusions in this study bracket the $^{87}Sr/^{86}Sr$ obtained pillow glasses from each volcano: the lowest $^{87}Sr/^{86}Sr$ in the melt inclusions (0.704858) is somewhat lower than the lowest value measured in whole rocks and pillow glasses (0.705352) from these two seamounts, and the highest $^{87}Sr/^{86}Sr$ in the melt inclusions (0.709225) is slightly higher than the highest value measured in pillow glasses (0.708901). This statement is also true for the $(La/Sm)_N$ and K_2O/TiO_2 for the melt inclusions compared to the whole rocks and pillow glasses (Fig. 4). Therefore, the Malumalu and Vailulu'u melt inclusions from these two hand samples represent the full compositional range previously identified in these volcanoes and, in fact, span nearly the entire range encountered in $^{87}Sr/^{86}Sr$ (i.e., 0.7045 to 0.7089) for the eastern Samoan volcanic province—including Ta'u, Vailulu'u, and Malumalu volcanoes—examined by Workman et al. (2006). Thus, the melt inclusions can be used to interpret mantle source geochemical characteristics, including volatile budgets, of the volcanoes examined in Workman et al. (2006).

4.2. Volatiles

After omitting melt inclusions that have been contaminated, breached, affected by hydrogen diffusion, and have unreliable CO_2 analyses by Raman, the magmatic volatile content of the Samoan melt inclusions can be explored. Fig. 5 provides ratios (H_2O/Ce, CO_2/Nb, Cl/Nb, S/Gd, and F/Nd) of volatile (H_2O, CO_2, Cl, S, and F) to nonvolatile (Ce, Nb, Gd, and Nd) incompatible trace elements (ITEs) that have similar mineral-melt partition coefficients during mantle melting and magmatic differentiation processes. Below we examine the volatile concentrations and their ratios to nonvolatile ITEs.

4.2.1. CO_2 in Samoan melt inclusions

We use the CO_2 concentration in the melt inclusion glass analyzed by SIMS and the CO_2 density in the vapor bubble from Raman spectroscopy to reconstruct the total CO_2 concentration of the melt inclusion. When comparing melt inclusion and vapor bubble CO_2, 3 to 94 mass percent (average ~59 mass percent) of the total CO_2 (i.e., melt inclusion CO_2 + vapor bubble CO_2) resides in the vapor bubble, consistent with prior findings of large CO_2 fractions residing in melt inclusion vapor bubbles (e.g., DeVitre et al., 2021; Aster et al., 2016; Moore et al., 2015). Malumalu and Vailulu'u melt inclusions have relatively similar total CO_2 contents of 1506–5746 ppm and 658–4771 ppm, respectively. The associated host pillow glasses for the Malumalu and Vailulu'u samples have total CO_2 contents of 70 ppm and 179 ppm, respectively (Workman et al., 2006), which is far lower than the melt inclusions from these two volcanoes. These observations are consistent with greater CO_2-H_2O saturation pressures for the melt inclusions than the pillow glasses.

During melting and crystallization, the incompatibility (i.e., the bulk partition coefficient) of CO_2 is similar to Nb and Ba, thus the ratios of CO_2/Nb or CO_2/Ba have been used to estimate upper mantle carbon content (Hirschmann, 2018; Michael and Graham, 2015; Saal et al., 2002; Cartigny et al., 2008; Le Voyer et al., 2017). However, only undegassed, CO_2-undersaturated melts will have CO_2/Nb or CO_2/Ba that are representative of the mantle source, but such melts are rare (Hauri et al., 2018; Graham and Michael, 2021; Le Voyer et al., 2017; Michael and Graham, 2015; Saal et al., 2002). These CO_2-undersaturated melts tend to be geochemically depleted (Hauri et al., 2018; Shimizu et al., 2023) and have higher CO_2/Nb than most submarine volcanic glasses, which are CO_2-saturated and thus degassed (e.g., the Samoan pillow glasses and melt inclusions examined here). With partially degassed melts, the best estimate for primary magmatic CO_2 comes from the highest CO_2/Nb (or CO_2/Ba) ratio of a melt inclusion suite or submarine glass suite (Matthews et al., 2017; Rosenthal et al., 2015). The Samoan melt inclusions in this study have a measured CO_2/Nb range of 19 to 125 for Vailulu'u melt inclusions and 27 to 133 for Malumalu melt inclusions, and such ratios are lower than inferred for mantle sources of oceanic hotspot lavas (e.g., >1000 for Iceland; Matthews et al., 2021) and MORB (CO_2/Nb > 283; Michael and Graham, 2015). Thus, we suggest the Samoan samples are CO_2-saturated and degassed, which is consistent with highly variable total CO_2 contents (658 to 5746 ppm) relative to the narrow range of Nb concentrations (26.3–55.8 ppm) in our Samoan melt inclusions (Fig. S6b,d). The Samoan pillow glasses from these two volcanoes have even lower (more degassed) CO_2 concentrations while exhibiting similar Nb concentrations to the melt inclusions (Fig. S6b,d).

4.2.2. Cl in Samoan melt inclusions versus Samoa pillow glasses

Malumalu melt inclusions have 651–1198 ppm Cl, and Vailulu'u melt inclusions have 412–765 ppm Cl (excluding the high Cl inclusion AVON3-71-2#14, which has a Cl concentration of 1.9 wt% Cl). The associated pillow glasses from the two samples hosting the melt inclusions—AVON3-78-1 and AVON3-71-2—have 1004 ppm Cl and 1490 ppm Cl, respectively. The suite of pillow glasses from all Malumalu and Vailulu'u samples have Cl contents that vary from 886 to 1725 ppm and 547 to 1818 ppm, respectively.

To determine if any melt inclusions are influenced by the assimilation of seawater-derived materials, we use Cl/Nb as an indicator of assimilation of seawater-derived materials (e.g., Kendrick et al., 2013, 2015; Kent et al., 1999a, 1999b, 2002). This is a useful ratio because Cl and Nb behave similarly during crystal fractionation and melting due to their similar incompatibility in basalt melts (Rowe and Lassiter, 2009). Malumalu melt inclusions have a Cl/Nb range of 14–25 and Vailulu'u melt inclusions have a Cl/Nb range of 14–22 (excluding melt inclusion sample AVON3-71-2#14, which has with Cl/Nb = 840) (Fig. 5). The Samoan melt inclusions have Cl/Nb that overlap with mid-ocean ridge

CORRECTED PROOF

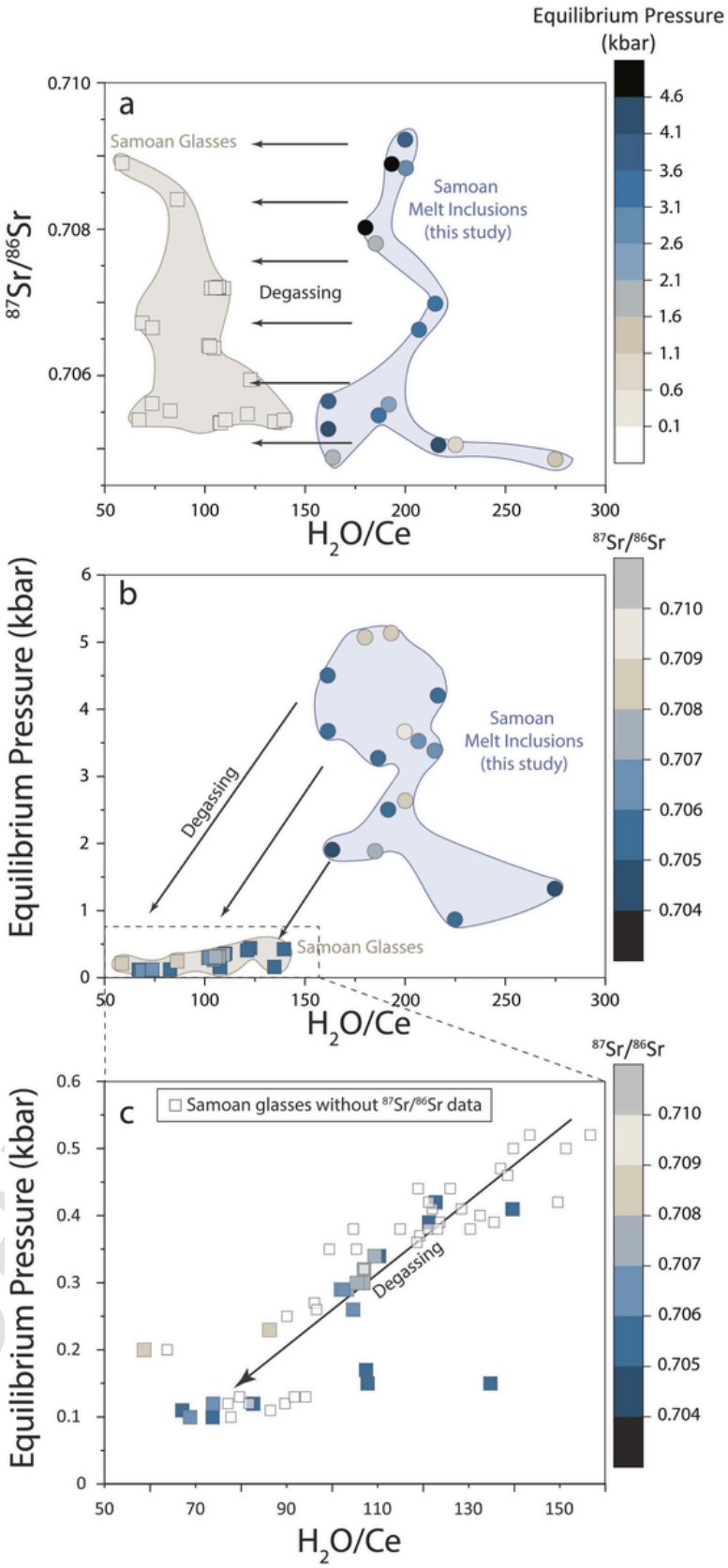

Fig. 3. $^{87}Sr/^{86}Sr$, H_2O/Ce, and equilibrium pressure for submarine pillow glasses from Malumalu and Vailulu'u seamounts are compared with melt inclusions from Malumalu sample AVON3-78-1 and Vailulu'u sample AVON3-71-2. (a) $^{87}Sr/^{86}Sr$ versus H_2O/Ce for Samoan melt inclusions and glasses with the color bar representing equilibrium pressure (kbar). The pillow glass data show separation in H_2O/Ce from the melt inclusion data, even though both datasets span a similar range in

Fig. 3.—*continued*
$^{87}Sr/^{86}Sr$. Circles represent melt inclusions and squares represent Samoan pillow glasses from Workman et al. (2006). Melt inclusions in this figure do not include any volatile-compromised melt inclusions (as shown in Fig. 2). VESIcal was used to calculate the equilibrium pressure of pillow glasses and melt inclusions using MagmaSat (Ghiorso and Gualda, 2015; Iacovino et al., 2021; Wieser et al., 2022) assuming temperature (1200 °C). Samoan pillow glass data are from Workman et al. (2006), except major elements used to calculate equilibrium pressure for AVON3-71-2 and AVON3-78-1 (which are from Kendrick et al., 2015). (b) Equilibrium pressure versus H_2O/Ce for Samoan melt inclusions and pillow glasses with the color bar representing $^{87}Sr/^{86}Sr$. (c) Expanded view of panel b that shows equilibrium pressure versus H_2O/Ce for Samoan pillow glasses only. Smaller square data points with black outlines are pillow glasses lacking $^{87}Sr/^{86}Sr$ data. Only samples with CO_2-H_2O saturation pressures ≥0.1 kbar are shown (just one Samoan glass with $^{87}Sr/^{86}Sr$ data has a saturation pressure < 0.1 kbar, sample AVON3-68-03 Rpt, so its removal does not significantly impact the dataset).

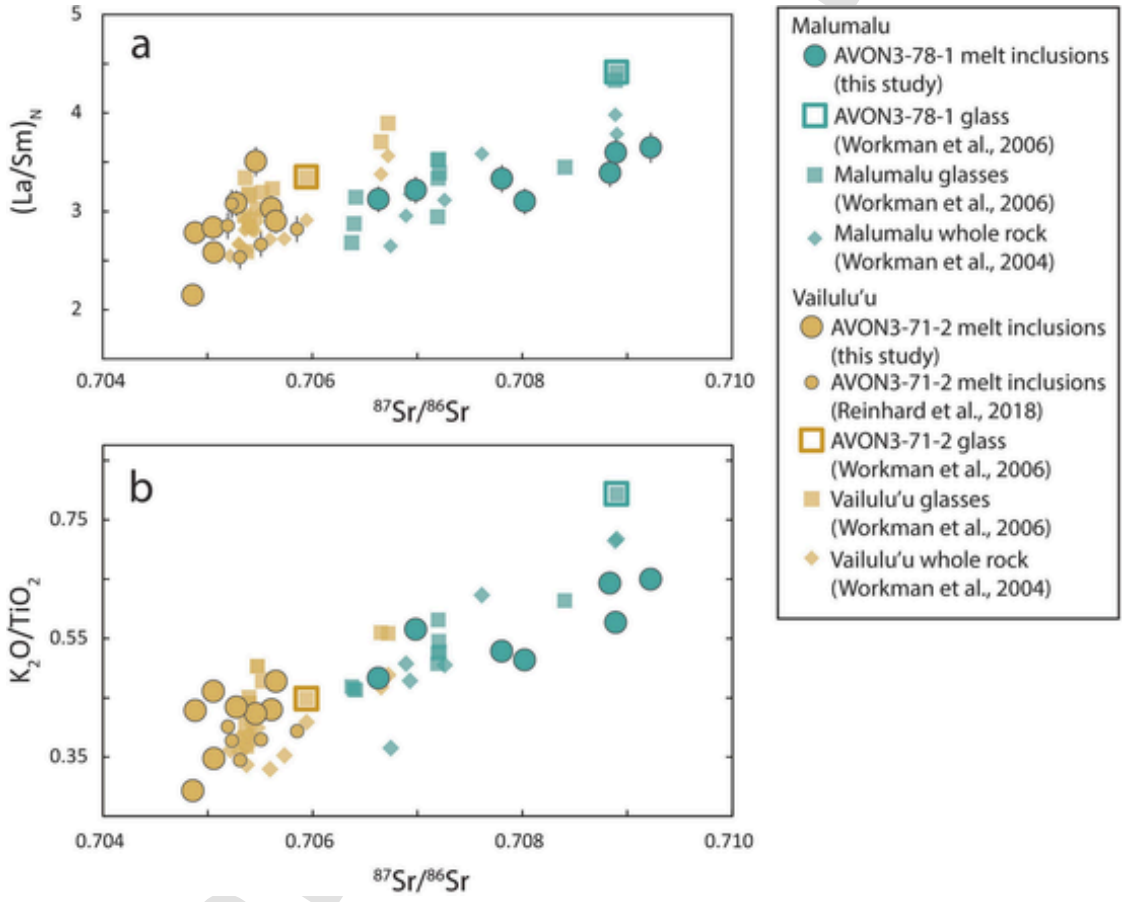

Fig. 4. Incompatible trace element ratios versus $^{87}Sr/^{86}Sr$ are shown for Samoan pillow glasses from Malumalu and Vailulu'u seamounts and new melt inclusion data from Malumalu sample AVON3-78-1 and Vailulu'u sample AVON3-71-2. The melt inclusions have incompatible trace element ratios and $^{87}Sr/^{86}Sr$ compositions that fall within the range identified in Samoan pillow glasses, indicating that the Samoan melt inclusions sample melts represented by the pillow glass dataset. (a) $(La/Sm)_N$ versus $^{87}Sr/^{86}Sr$, where N signifies normalization to primitive mantle (McDonough and Sun, 1995). (b) K_2O/TiO_2 versus $^{87}Sr/^{86}Sr$. Data for Samoan pillow glasses are from Workman et al. (2006) and Kendrick et al. (2015). Error bars for La/Sm (4.2%) are shown for the melt inclusions and are calculated as $((La\ error)^2 + (Sm\ error)^2)^{0.5}$, where the 2RSD of the secondary standard BCR-2 is used for La error (1.9%) and Sm error (3.8%) (see Table S2). Error bars on K_2O/TiO_2 are smaller than the data symbols. Melt inclusions that are compromised with respect to their volatile contents are not shown.

basalts (MORB), where Cl/Nb_{MORB} is 5 to 17 (Lassiter et al., 2002; Le Roux et al., 2006), but the Samoan inclusions tend to be shifted to higher Cl/Nb.

The pillow glasses for the Malumalu (AVON3-78-1) and Vailulu'u (AVON3-71-2) samples hosting the Samoan melt inclusions have Cl/Nb of 13 and 27, respectively (Kendrick et al., 2015). Both lavas have been previously suggested to have assimilated seawater-derived materials (Kendrick et al., 2014; Reinhard et al., 2018). We find some evidence for assimilation in a single melt inclusion from Vailulu'u (AVON3-71-2#14), which has a high Cl/Nb ratio of 840, suggesting contamination by seawater-derived materials; however, any such assimilation does not appear to have impacted $^{87}Sr/^{86}Sr$ (0.705471 ± 0.000022) as it is at the lower end of the range observed here (Fig. 5).

4.2.3. S in Samoan melt inclusions versus Samoa pillow glasses

Malumalu melt inclusions have 1786–3163 ppm S, and Vailulu'u melt inclusions have 1582–2090 ppm S. The associated host pillow glasses (AVON3-78-1 and AVON3-71-2) have 831 ppm S and 2337 ppm S, respectively. The suite of pillow glasses from all Malumalu and Vailulu'u samples have S contents varying from 781 to 2391 ppm and 1010 to 4834 ppm, respectively (Workman et al., 2006).

Sulfur and Gd and Dy have similar incompatibility during melting and crystal fractionation (Saal et al., 2002) when sulfide is not present, except at lower pressures when sulfur degasses. However, Samoan basalts are known to host both sulfates and sulfides (Labidi et al., 2015). The melt inclusions in this study are sulfide-saturated (Fig. S5; using the model of Fortin et al., 2015 and Smythe et al., 2017)—and sulfides are in fact, observed in some of the inclusions from the two samples examined here —thus S/Gd (Fig. 5) of Samoan melt inclusions

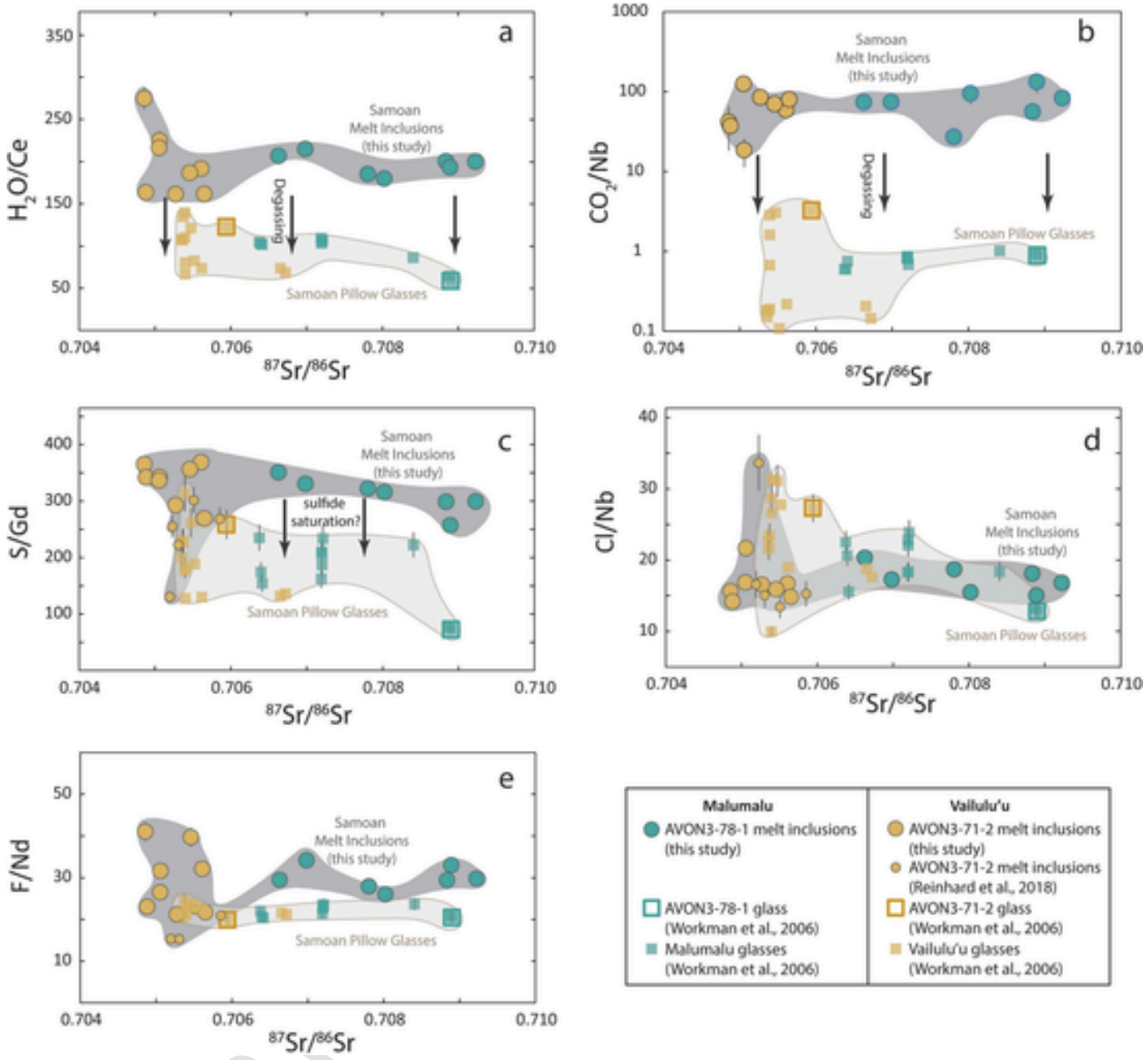

Fig. 5. Element ratios (volatile/incompatible trace element) are plotted against $^{87}Sr/^{86}Sr$ for Samoan pillow glasses from Malumalu and Vailulu'u seamounts and the new melt inclusion data from Malumalu sample AVON3-78-1 and Vailulu'u sample AVON3-71-2. See Supplementary Text section S1.6 for a discussion on the calculation of the errors associated with the element ratios presented here; the error bars for the $^{87}Sr/^{86}Sr$ of Samoan glasses and melt inclusions are smaller than the symbol size. Melt inclusions that are compromised with respect to their volatile contents (as shown in Fig. 2) are not shown. Only samples with CO_2-H_2O saturation pressures ≥0.1 kbar are shown (just one Samoan glass with $^{87}Sr/^{86}Sr$ data has a saturation pressure < 0.1 kbar, sample AVON3-68-03 Rpt, so its removal does not significantly impact the dataset).

in this study may have been influenced by sulfide saturation and are likely not representative of the Samoan primary melts.

4.2.4. F in Samoan melt inclusions versus Samoa pillow glasses

Malumalu melt inclusions have 1161–1293 ppm F, and Vailulu'u melt inclusions have 777–1145 ppm F. The associated host pillow glasses (AVON3-78-1 and AVON3-71-2) have 1254 ppm F and 903 ppm F, respectively. The suite of pillow glasses from all Malumalu and Vailulu'u samples have F contents varying from 1173 to 1409 ppm, and 843 to 1188 ppm F, respectively (Workman et al., 2006).

F/Nd in melt inclusions and glasses from global datasets of MORB and OIB are suggested to be relatively constant because there is no significant F/Nd fractionation during crystallization and melting. The F/Nd values of global OIB and MORB have been estimated to be 20.1 ± 5.8 (Workman et al., 2006), but there is evidence for greater F/Nd variability (Koleszar et al., 2009; Shimizu et al., 2016; Jackson et al., 2015; Lassiter et al., 2002; Métrich et al., 2014; Cabral et al., 2014; Rose-Koga et al., 2012). The average F/Nd for Malumalu melt inclusions (30 ± 6 2SD, N = 8) is similar to the average F/Nd for Vailulu'u melt inclusions (29 ± 14 2SD, N = 10), but Vailulu'u melt inclusions have more variability in F/Nd (Fig. 5). Three Vailulu'u melt inclusions (AVON3-71-2#7, #17, #22) have ~200 ppm lower F contents than the other Samoan melt inclusions, but similar Nd contents, resulting in lower F/Nd (21–23). The Samoan melt inclusion have F/Nd (30 ± 11, 2SD, N = 18) tends to be higher than the canonical F/Nd (~21) for fresh global OIB and MORB, and higher than the average pillow glass F/

Nd from Malumalu (22 ± 2, 2SD, N = 17; Workman et al., 2006) and Vailulu'u (22 ± 3, 2SD, N = 48; Workman et al., 2006). However, the average F/Nd of Samoan melt inclusions overlaps within two standard deviations of the canonical F/Nd value and the F/Nd of Samoan pillow glasses. Nonetheless, the Vailulu'u melt inclusions tend to very high F/Nd up to 41. Elevated F may be characteristic of the HIMU mantle source (Hauri and Hart, 1993; Rose-Koga et al., 2017; Jackson et al., 2015), and Vailulu'u is thought to contain a small contribution from a HIMU component (Workman et al., 2004; Jackson et al., 2014). However, we do not have an explanation for the higher F/Nd in the Vailulu'u melt inclusions relative to the glasses from this seamount.

4.2.5. H_2O in Samoan melt inclusions versus Samoa pillow glasses

Malumalu melt inclusions have 1.56–1.95 wt% H_2O, and Vailulu'u melt inclusions have 1.13–1.39 wt% H_2O. The associated host glasses from these two submarine samples tend to have lower H_2O contents than the melt inclusions with 0.91 wt% H_2O (AVON3-78-1) and 1.18 wt% H_2O (AVON3-71-2), respectively. The low H_2O in the AVON3-78-1 Malumalu glass sample lies within the range of H_2O for pillow glass samples from Malumalu (0.89 to 1.43 wt%), and the same applies for the AVON3-71-2 Vailulu'u glass sample as it also lies in the range of pillow glasses from this seamount (0.63 to 1.50 wt%) (Fig. 6). When the melt inclusions and pillow glasses are corrected for olivine fractionation to be in equilibrium with mantle olivine (Fo_{90}), a figure of H_2O_{Fo90} (wt%) versus Ce_{Fo90} (ppm) shows that the melt inclusions and pillow glasses from Malumalu and Vailulu'u seamounts have similar

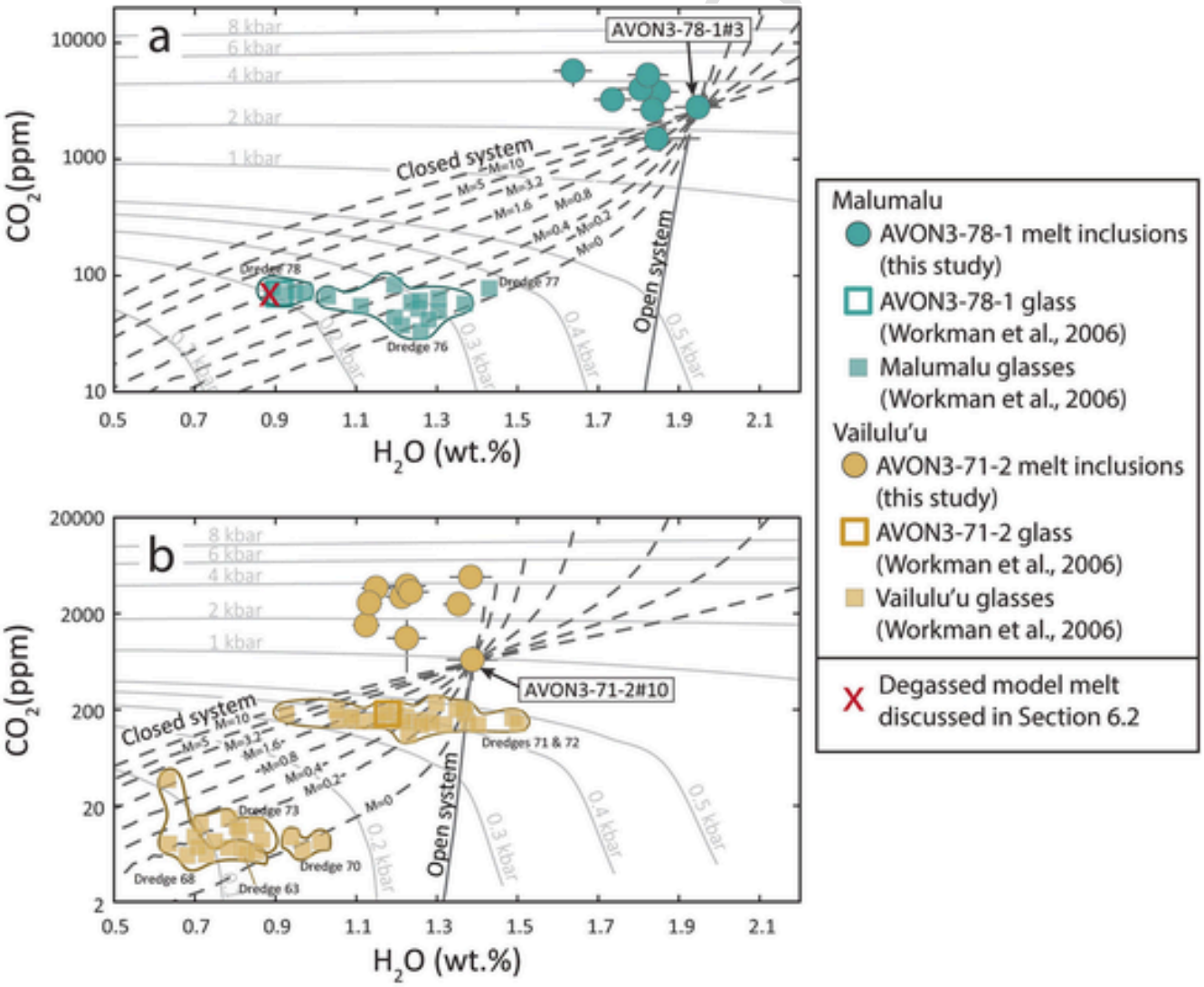

Fig. 6. CO_2 (ppm) versus H_2O (wt%) for (a) melt inclusions from Malumalu sample AVON3-78-1 and all pillow glasses from Malumalu seamount and (b) melt inclusions from Vailulu'u sample AVON3-71-2 and all pillow glasses from Vailulu'u seamount. Melt inclusion data are from this study and Samoan pillow glass data are from Workman et al. (2006) and the data are shown in fields separated by the dredge number (which is provided next to the relevant field). Isobars are calculated using MagmaSat for an average melt inclusion composition of each sample at 1200 °C. Closed-system degassing curves are calculated with varying values for M (where "M" represents mass fraction of equilibrium fluid in the magma but here is given as a percentage; e.g., M = 1.6 means there was 1.6 wt% of fluid in the magma before degassing). Degassing trends assume an oxygen fugacity (QFM) and temperature (1200 °C) and are calculated in rhyolite-MELTS v1.2 using H_2O and CO_2 compositions that match the highest H_2O melt inclusions in the respective panels (i.e., Malumalu melt inclusion AVON3-78-1#3 in the upper panel, and Vailulu'u melt inclusion AVON3-71-2#10 in the lower panel); other compositions used in the degassing calculation are in Table S9. Melt inclusion CO_2 and H_2O concentrations shown are values that have been corrected to be in equilibrium with the host olivine. Volatile-compromised melt inclusions (as shown in Fig. 2) are not included in this figure. Other parental melt compositions are possible as initial values for the degassing model, but for simplicity, we use the highest H_2O inclusions because they allow the degassing model to encompass the pillow glasses with the highest H_2O concentrations.

Ce_{Fo90}, but the inclusions have H_2O that is higher than the pillow glasses (Fig. S6c). We also show the same plot but instead provide the *measured* H_2O and Ce in the glass glasses—due to uncertainties associated with the olivine correction—and find that it does not change our conclusions.

Consistent with this observation, the H_2O/Ce range of the Malumalu AVON3-78-1 melt inclusions (180–232, average 202 ± 33, 2SD, N = 8) and the Vailulu'u AVON3-71-2 melt inclusions (161–275, average 190 ± 78, 2SD, N = 10) are higher than the host pillow glasses, 59 (for pillow glass from sample AVON3-78-1) and 123 (for pillow glass from sample AVON3-71-2), respectively. Critically, the average H_2O/Ce (197 ± 58 2SD, N = 15) in the melt inclusion dataset from Malumalu and Vailulu'u seamounts is nearly twice as high as the same ratio in the Samoan pillow glasses from these two seamounts (106 ± 51, 2SD, N = 65). This is notable because the inclusions and pillow glasses are from the same two volcanoes, span the same range of $^{87}Sr/^{86}Sr$ (Fig. 3), and have similar ITE ratios (Fig. 4), suggesting they sample the same mantle sources. This observation that melt inclusions have higher H_2O/Ce than submarine pillow glasses may relate to the fact that the Samoan melt inclusions from Malumalu and Vailulu'u have universally higher calculated MagmaSat CO_2-H_2O vapor saturation pressures (Fig. 3) than the submarine pillow glasses, reflective of higher entrapment pressures for the melt inclusions (>0.870 kbar) than the eruption pressures experienced by the glasses (<0.53 kbar) (see Fig. 3).

While Workman et al. (2006) found a negative correlation between H_2O/La and $^{87}Sr/^{86}Sr$ for Samoan glasses, we find that the Samoan melt inclusions in this study exhibit *no correlation* between H_2O/Ce and $^{87}Sr/^{86}Sr$ (Figs. 3, 5a, 7a), even though the melt inclusions are from two of the three volcanoes studied by Workman et al. (2006) and span the same range of $^{87}Sr/^{86}Sr$ as their pillow glasses. In contrast to Workman et al. (2006), the H_2O/Ce of the melt inclusions is quite constant (i.e., 197 ± 58 2SD, N = 15) over a range of $^{87}Sr/^{86}Sr$ from 0.704858 to 0.709225, and the melt inclusions with the strongest EM2 mantle signatures (i.e., $^{87}Sr/^{86}Sr$ > 0.7080, N = 4) have elevated H_2O/Ce (193 ± 19 2SD) that is indistinguishable from the H_2O/Ce (202 ± 31) in melt inclusions with weaker EM2 signatures ($^{87}Sr/^{86}Sr$ < 0.7080, N = 3).

While the Samoan pillow glasses and melt inclusions exhibit some overlap with each other in H_2O/Ce at the lowest $^{87}Sr/^{86}Sr$, they exhibit diverging trends in H_2O/Ce with increasing $^{87}Sr/^{86}Sr$: melt inclusions exhibit unchanging H_2O/Ce with increasing $^{87}Sr/^{86}Sr$, and glass exhibit decreasing H_2O/Ce with increasing $^{87}Sr/^{86}Sr$. Thus, the difference in H_2O/Ce between melt inclusions and glasses is largest at the highest $^{87}Sr/^{86}Sr$ (Fig. 7). To illustrate this, we note that all four pillow glasses with the strongest EM2 signatures ($^{87}Sr/^{86}Sr$ > 0.7080) have H_2O/Ce < 90 (H_2O/Ce average of 75 ± 30, 2SD) while the H_2O/Ce of the four melt inclusions with the highest $^{87}Sr/^{86}Sr$ (>0.7080) have H_2O/Ce that is more than twice as high as that in the pillow glasses (H_2O/Ce average of 193 ± 19, 2SD). Prior studies (e.g., Workman et al., 2006) often cite that pillow glasses erupted at depths >1000 mbsl retain volatile/ITE ratios of the mantle source. All pillow glasses shown in Fig. 7 have H_2O-CO_2 saturation pressures ≥0.1 kbar. Given that the melt inclusions and glasses in Fig. 7 exhibit deep saturation pressures and appear to sample the same mantle source (Fig. 4), we might expect the deeply-erupted pillow glasses should have the same H_2O/Ce as melt inclusions. These observations raise a key question that we will address in the discussion: why do melt inclusions and pillow glasses erupted at depths >1000 mbsl from the same volcanoes and with the same $^{87}Sr/^{86}Sr$ (i.e., sampling the same mantle sources) have H_2O/Ce that differ, on average, by nearly a factor of two?

5. Modeling degassing processes for Samoan melts

We find that melt inclusions from the Vailulu'u and Malumalu seamounts have higher CO_2 concentrations than their corresponding pillow glasses (Fig. 6), indicating that the deeply-erupted submarine pillow glasses are more degassed than the melt inclusions. An outstanding question is whether the lower H_2O/Ce in the pillow glasses reflects this higher degree of degassing via concomitant degassing of both CO_2 *and* H_2O.

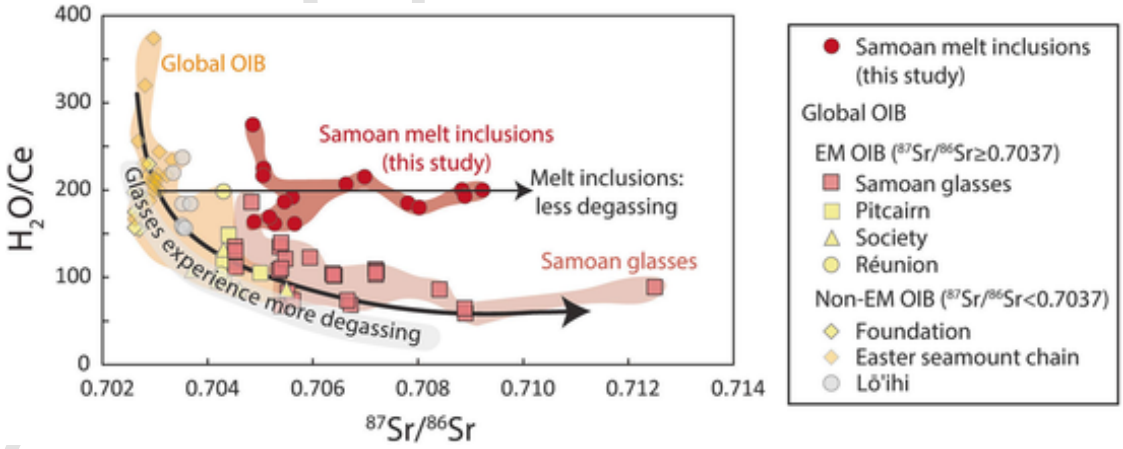

Fig. 7. Samoan melt inclusions and pillow glasses compared to a global dataset of submarine OIB glasses. Samoan melt inclusions—protected from the extensive degassing experienced by Samoan pillow glasses—have higher H_2O/Ce than Samoan pillow glasses, and thus fall off of the global submarine OIB pillow glass trend that shows decreasing H_2O/Ce with increasing $^{87}Sr/^{86}Sr$. The arrows in this figure are merely schematic to guide the reader and are not the result of a model. Only OIB glasses with $^{87}Sr/^{86}Sr$ (to establish the level of source enrichment) and MgO > 4.5 wt% (to minimize the impact of fractional crystallization) are shown. Sources of data (see Table S11): Pitcairn (Kendrick et al., 2014; Woodhead and Devey, 1993), Society (Devey et al., 1990; Kendrick et al., 2014), Réunion (Kendrick et al., 2017; Fretzdorff and Haase, 2002), Foundation (Kendrick et al., 2017), Easter seamount chain (Dixon et al., 2002), Lō'ihi (Dixon and Clague, 2001; Staudigel et al., 1984). Samples from Pitcairn, Society, Réunion, and Foundation can be found in a data compilation by Kendrick et al. (2017). Samples marked as having experienced assimilation of seawater Cl in Kendrick et al. (2017) are excluded. However, unlike Dixon et al. (2002), we do not use H_2O/Ce as a filter for assimilation. Samoan pillow glasses include submarine glasses characterized for $^{87}Sr/^{86}Sr$ from Vailulu'u, Malumalu, Tupito (formerly known as Muli), Taumatau, and Ta'u (Kendrick et al., 2015; Workman et al., 2006). Volatile-compromised melt inclusions (as shown in Fig. 2) are not shown. Melt inclusions from other OIB localities are not shown because there are no other OIB melt inclusions characterized for both $^{87}Sr/^{86}Sr$ and H_2O/Ce. Only samples with CO_2-H_2O saturation pressures ≥0.1 kbar are shown (just one Samoan glass with $^{87}Sr/^{86}Sr$ data has a saturation pressure <0.1 kbar, sample AVON3-68-03 Rpt, so its removal does not significantly impact the dataset).

We show that the data are consistent with Samoan pillow glasses being related to the Samoan melt inclusions through closed-system degassing; the new insight gained here is that, when compared with genetically-related melt inclusions, it is clear that even deeply erupted glasses (with CO_2-H_2O saturation pressures ≥0.1 kbar) have lost significant H_2O and have lower H_2O/Ce compared to their primary melt (Fig. 3). This is evident in models we have run using a set of open- and closed-system degassing paths while also varying the fraction of CO_2 + H_2O fluid in equilibrium with the initial melt (Fig. 6).

There are indications that there is a volatile-bearing fluid phase coexisting with magma in magma reservoirs at depths before eruption (e.g., CO_2 fluxing: Rust et al., 2004; Blundy et al., 2010). Therefore, a free parameter M is introduced, representing the mass fraction of a volatile fluid in the magma + fluid system (e.g., VESIcal program has this parameter built-in; Iacovino et al., 2021; Wieser et al., 2022). In this case, $[CO_2]$ in the system = $(1-M)([CO_2]_{melt\ observed})$ + $M([CO_2]_{equilibrium\ fluid})$. A similar equation is also used for H_2O. In the models, we define the variable M as the mass fraction of fluid (shown as a percentage in Fig. 6) in equilibrium with the melt, where M = 0% means that no initial fluid is in equilibrium with the melt (i.e., all volatiles are dissolved in the melt, no fluid is present in excess), and where M = 100% means that all volatiles are in the fluid (i.e., no melt is present). The higher the M value, the deeper degassing starts (Fig. S8). We generate degassing paths assuming a starting H_2O and CO_2 composition equivalent to the melt inclusion with the highest H_2O content from Malumalu seamount (sample AVON3-78-1#3) to model Malumalu data, and the equivalent high-H_2O melt inclusion from Vailulu'u (sample AVON3-71-2#10) to model Vailulu'u data. We use MagmaSat (Ghiorso and Gualda, 2015) to calculate the fluid composition (i.e., XCO_2 and XH_2O) in equilibrium with the two melt inclusions (see Table S9 for model melt inclusion compositions). Additionally, we use rhyolite-MELTS v.1.2 (which incorporates the same fluid solubility model as MagmaSat) in rhyolite-MELTS to simulate degassing because this model is well-suited for high CO_2 contents in the initial melt composition (Ghiorso and Gualda, 2015; Gualda et al., 2012). The models are run at 1200 °C, and start at 3–27 kbar, and run to 1 bar. The influence of oxygen fugacity on the model degassing path is negligible, so we assume QFM for all models. The compositional and physical parameters used in the MagmaSat and rhyolite-MELTS models are given in Table S9.

The degassing model results are presented in Fig. 6. While there is no single degassing path that explains the difference in pillow glass and melt inclusion CO_2 and H_2O concentrations, closed-system degassing paths with M values ranging from 0% to 10% describe most of the pillow glasses from both seamounts. However, there are some Vailulu'u pillow glasses that have H_2O that is higher than the range described by the calculated degassing paths. For example, three Vailulu'u pillow glasses have higher H_2O concentrations than the highest-H_2O melt inclusion. This could be because the melt inclusion suite in this study does not represent the full range of H_2O contents possible at the seamount, and higher initial H_2O concentrations may be more reflective of the primary melts.

A primary observation from this modeling exercise is that closed-system degassing from melt inclusion entrapment pressures (i.e., > 0.87 kbar) to eruption on the seafloor (pillow glasses have equilibrium pressures of 0.08 to 0.53 kbar) results in significant loss of both CO_2 *and* H_2O, even for glasses with CO_2-H_2O saturation depths near 0.4 kbar (see closed-system degassing paths in Fig. 6). Furthermore, the presence of equilibrium fluid (M) indicates that the magmatic system is richer in CO_2, and thus starts to degas at greater depths. Below we show that loss of H_2O during closed-system degassing to shallow levels (i.e., <0.53 kbar) explains the lower H_2O/Ce in pillow glasses compared to the melt inclusions.

6. Discussion

H_2O has incompatibility during mantle melting similar to Ce (Michael, 1995), thus H_2O/Ce of the melt inclusions and glasses should reflect the mantle source unless the samples have degassed. Clear negative correlations between H_2O/Ce and $^{87}Sr/^{86}Sr$ in pillow glasses have been used to infer the H_2O/LREE (light rare earth element) ratios of the mantle source, assuming the H_2O has not been degassed. The primary observation in this study that we seek to explain is that Samoan pillow glasses and olivine-hosted melt inclusions span the same range of $^{87}Sr/^{86}Sr$ and incompatible trace element ratios unaffected by differentiation—and thus sample the same mantle sources, yet the melt inclusions have H_2O/Ce ratios that are approximately twice as high as the pillow glasses. The second key observation is that the melt inclusion H_2O/Ce ratios are relatively constant over a wide range of $^{87}Sr/^{86}Sr$, in contrast to the pillow glasses whose H_2O/Ce ratios anticorrelate with $^{87}Sr/^{86}Sr$. This raises two key questions: Why do Samoan EM2 pillow glasses exhibit H_2O/Ce that are approximately half the values in Samoan EM2 melt inclusions at the same seamounts, and what does this mean for the H_2O content of the EM2 mantle?

6.1. Higher H_2O/Ce in melt inclusions relative to pillow glasses: Diffusive H_2O gain through host olivine and/or assimilation of seawater-derived materials?

In order to compare the volatile contents of the Samoan melt inclusions and pillow glasses in this study, it is important to assess whether the higher H_2O/Ce in the inclusions reflects processes operating in the magma during ascent, such as diffusive proton gain (i.e., addition of H) or assimilation of seawater-derived materials. Prior work has shown that, compared to large melt inclusions, small inclusions are more susceptible to diffusive loss or addition of protons, and this results in modified δD (Hauri, 2002; Portnyagin et al., 2008; Gaetani et al., 2012; Bucholz et al., 2013; Hartley et al., 2015). Given enough time, the δD of all inclusions will eventually equilibrate with the external melt. Diffusive proton loss from the inclusion can be identified by an increase in δD, which is associated with decreasing melt inclusion volume. Conversely, diffusive gain of protons by the inclusion is identified by a decrease in δD, where the magnitude of the δD reduction is greater in the smaller volume melt inclusions. The new δD analyses on melt inclusions show a lack of variation in δD (−35.9 ± 17.4‰, 2SD, N = 18) with melt inclusion size for melt inclusions with volumes >10^5 μm³, which indicates no water loss or gain in the larger inclusions (Fig. 2). However, the two smallest melt inclusions (AVON3-78-1#13 and AVON3-78-1#32), both with melt inclusion volume <10^5 μm³, have significantly higher δD (+128‰ and +6 ‰, respectively) than the other melt inclusions from this lava, which indicates that the small volume melt inclusions have experienced diffusive H_2O loss, not H_2O addition (Fig. 2). These two small volume inclusions are excluded from the discussion below. While there is a lack of variation in δD, the variability in H_2O concentrations of the melt inclusions in both seamounts does not suggest that diffusion has fully overprinted the original H_2O concentration of the melt inclusions. Additionally, the variability in H_2O concentrations across the melt inclusions from a single sample (AVON3-78-1 or AVON3-71-2) does not relate to melt inclusion size, which indicates that the variability in H_2O is independent of H diffusive exchange with the host melt.

Assimilation of seawater-derived materials can increase H_2O in magmas (except if the magma is saturated in H_2O), and this process can be traced by monitoring Cl/Nb, a ratio that is elevated in seawater-derived materials. One hypothesis for the higher H_2O/Ce in melt inclusions is that they have experienced more assimilation of seawater-derived materials compared to Samoan pillow glasses, and this hypothesis can be tested by measurement of $^{87}Sr/^{86}Sr$. A plot of Cl/Nb versus

CORRECTED PROOF

$^{87}Sr/^{86}Sr$ shows that Samoan pillow glasses and melt inclusions have an overlapping range of Cl/Nb at any given $^{87}Sr/^{86}Sr$, so the offset to higher H_2O/Ce in the melt inclusions is not explained by greater assimilation experienced by melt inclusions (Fig. 5). We do acknowledge that one melt inclusion with exceptionally high Cl/Nb (840)—a ratio consistent with assimilation of seawater-derived materials (Table S1)—also has elevated H_2O/Ce (366), suggesting a role for assimilation in increasing the H_2O/Ce in this particular inclusion. However, this single inclusion has been excluded from the discussion below owing to its very high Cl/Nb.

In short, diffusive gain of H_2O and preferential assimilation of seawater-derived materials by the melt inclusions relative to the pillow glasses do not explain the higher H_2O/Ce in the melt inclusions relative to the pillow glasses. Instead, we argue in the following section that closed-system degassing plays a key role in lowering the H_2O and the H_2O/Ce of pillow glasses. In contrast, limited H_2O degassing has occurred in the melt inclusions in this study, leaving the melt inclusion H_2O/Ce relatively unchanged (although there may have been some H_2O loss prior to entrapment in crystallizing olivines), thereby explaining why melt inclusions have higher H_2O/Ce than pillow glasses. This contrasts with prior studies (e.g., Workman et al., 2006) suggesting that pillow glasses erupted at depths >1000 mbsl retain H_2O/LREE ratios of the mantle source.

6.2. Higher H_2O/Ce in melt inclusions relative to pillow glasses: H_2O loss in Samoan glasses caused by degassing

We argue that the difference in H_2O/Ce between Samoan EM2-flavored melt inclusions and pillow glasses from the same seamounts relates to greater degassing of the pillow glasses relative to the melt inclusions. Unlike the pillow glasses, which can experience degassing from great depth all the way to eruption and quenching on the seafloor, melt inclusions trap melts at magma chamber depths and act as pressure vessels, which inhibits degassing at shallower levels during magma ascent. To evaluate this hypothesis, we build on the indistinguishable $^{87}Sr/^{86}Sr$ and nonvolatile incompatible trace element ratios between pillow glasses and melt inclusions and argue that, at the depth of melt inclusion entrapment, the H_2O/Ce of the melts that later erupted as Samoan pillow glasses was *also* the same as the Samoan melt inclusions (i.e., nonvolatile ITE ratios—which remain unmodified from primary melt compositions during fractional crystallization of magmas with MgO as high as identified in the data reported here (Fig. S1)—and $^{87}Sr/^{86}Sr$ data obtained on the melt inclusions indicate that they derive from the same parental melts as the pillow glasses and thus should have started with the same H_2O/Ce). The H_2O/Ce of the pillow glasses, but not the melt inclusions, was then lowered by H_2O degassing during ascent.

The hypothesis of H_2O loss from the matrix melts by degassing is supported by closed-system degassing models in Fig. 6. For example, the degassing model for Malumalu AVON3-78-1 starts with a melt inclusion composition like AVON3-78-1#3 which has an elevated CO_2 concentration of 2810 ppm, the highest H_2O concentration from this lava (1.95 wt%), and a high entrapment pressure of 2.63 kbar (i.e., the CO_2-H_2O saturation pressure calculated for the melt inclusion using MagmaSat). Closed-system degassing of this melt composition from 2.63 kbar to 0.2 kbar—the approximate CO_2-H_2O saturation pressure for the pillow glass from this lava, sample AVON3-78-1—at M = 1.6 lowers the water content by a factor of ~2.1 to 0.90 wt%, and the CO_2 content by a factor of ~40 to 69 ppm. The red "x" in Fig. 6a defines the CO_2 and H_2O composition of the model melt following degassing, and the degassed model melt is very similar in composition to the pillow glass sample AVON3-78-1 and helps explain the low H_2O (0.91 wt%) and CO_2 (70 ppm) of AVON3-78-1. This is important because this particular pillow glass sample anchors the highest $^{87}Sr/^{86}Sr$ (0.7089) and lowest H_2O/Ce (59) portion of the $^{87}Sr/^{86}Sr$ versus H_2O/Ce array produced by Workman et al. (2006) who interpreted that the low H_2O/Ce in this EM2 glass reflects melting of a water-poor ("dry") EM2 mantle. In contrast, we show that dramatic H_2O-loss during closed-system degassing of an ascending EM2 melt with an initially high H_2O/Ce ratio (H_2O/Ce = 200) is responsible for the low H_2O/Ce (59) in the AVON3-78-1 glass. This model contrasts with prior studies (e.g., Workman et al., 2006) suggesting that pillow glasses erupted at depths >1000 mbsl (≥0.1 kbar) retain the H_2O/LREE ratios of the mantle source.

We observe a relatively constant and elevated H_2O/Ce ratio in melt inclusions over a wide range of $^{87}Sr/^{86}Sr$—melt inclusions with strong EM2 mantle signatures (i.e., $^{87}Sr/^{86}Sr > 0.7080$) have elevated H_2O/Ce (193 ± 19 2SD, $N = 4$) that is indistinguishable from H_2O/Ce (202 ± 31, $N = 3$) in melt inclusions with weaker EM2 signatures ($^{87}Sr/^{86}Sr < 0.7080$). This also contrasts with Workman et al.'s (2006) observation that H_2O/LREE is lower in the Samoan EM2 pillow glasses with higher $^{87}Sr/^{86}Sr$. Unlike Workman et al. (2006), who argued that the low H_2O/LREE in Samoan EM2 glasses is a source feature, we show that the low ratio in these pillow glasses relative to that of the melt inclusions can be explained by closed-system degassing of magmas during ascent to the seafloor. If this degassing model is correct, and if Samoan high $^{87}Sr/^{86}Sr$ and low $^{87}Sr/^{86}Sr$ melts have the same initial H_2O/Ce—as supported by observations from melt inclusions in Fig. 5a—then the negative correlation between $^{87}Sr/^{86}Sr$ in H_2O/Ce in the pillow glasses in Workman et al. (2006) (Fig. 7) leads us to an important conclusion: the Samoan EM2 pillow glasses have degassed more H_2O (to achieve lower H_2O/Ce) than Samoan pillow glasses with weaker EM2 signatures (which have higher H_2O/Ce). Therefore, we next focus on identifying the mechanism that results in greater H_2O degassing in more extreme EM melts relative to non-EM melts.

6.3. Explaining the inverse relationship between $^{87}Sr/^{86}Sr$ and H_2O/Ce in global pillow glasses by degassing

The global OIB dataset on submarine pillow glasses exhibits an inverse relationship between $^{87}Sr/^{86}Sr$ and H_2O/Ce (Fig. 7) that is similar to the inverse correlation observed in Samoan submarine glasses, and it has long been known that submarine glasses with low $^{87}Sr/^{86}Sr$ tend to have higher H_2O/Ce than glasses with high $^{87}Sr/^{86}Sr$ (e.g., Dixon et al., 2002; Workman et al., 2006; Kendrick et al., 2014). The Samoan melt inclusions noticeably stray from this trend. The Samoan melt inclusions with high $^{87}Sr/^{86}Sr$ are shifted to higher, relatively constant H_2O/Ce (197 ± 58 2SD, $N = 15$) compared to the H_2O/Ce (108 ± 58, 2SD, $N = 41$) in a global database of OIB glasses (including Samoa) that have similarly high $^{87}Sr/^{86}Sr$ (i.e., >0.7037) (Fig. 7). In fact, the high H_2O/Ce of Samoan inclusions (197 ± 58 2SD, N = 15) is similar to the H_2O/Ce (209 ± 92, 2SD, $N = 32$) of pillow glasses characterized by low $^{87}Sr/^{86}Sr$ (<0.7037, the threshold value used to distinguish between EM and non-EM melts). If the Samoan melt inclusions represent less degassed versions of the melts sampled by Samoan submarine glasses, then the similarity in H_2O/Ce between low $^{87}Sr/^{86}Sr$ (<0.7037) OIB pillow glasses and Samoan melt inclusions (>0.7037) raises the possibility that non-EM OIB melts and EM OIB melts initially have the same H_2O/Ce, but the latter suffer more degassing of H_2O than the former during magma ascent. If the inverse correlation between H_2O/Ce and $^{87}Sr/^{86}Sr$ in Samoan, and global, OIB glasses is driven by greater degassing of the most geochemically enriched lavas compared to geochemically depleted lavas, what mechanism causes geochemically enriched glasses from OIB mantle sources to have suffered more H_2O degassing than geochemically depleted glasses?

Previous work suggests that EM mantle sources have higher CO_2, and generate primary melts with higher CO_2, than non-EM mantle sources (Burnard et al., 2014; Cartigny et al., 2008; Taracsák et al., 2019; Hauri et al., 2018; Miller et al., 2019; Matthews et al., 2021; Michael and Graham, 2015; Shimizu et al., 2023). We show that primary melts with higher CO_2 degas more CO_2 *and* more H_2O by closed-system degassing during ascent than primary melts with the same H_2O

CORRECTED PROOF

but lower CO_2 concentrations. As a result, EM lavas that were initially more CO_2-rich erupt on the seafloor with lower H_2O/Ce than their geochemically-depleted non-EM counterparts that started with lower primary melt CO_2, even though both EM and non-EM primary melts started with the same H_2O concentrations and H_2O/Ce. At the extreme end, non-EM (i.e., geochemically depleted) melts erupted at, for example, MORB settings, can have such low primary melt CO_2 that they never saturate and neither CO_2 nor H_2O are lost by degassing (Saal et al., 2002; Michael and Graham, 2015; Hauri et al., 2018).

By contrast, we argue that CO_2-rich primary melts, typical of geochemically-enriched OIB settings, saturate CO_2 at great depths and lose significant CO_2 and H_2O by closed-system degassing. In order to show this, we first estimate primary melt CO_2 for a suite of global OIB glasses using a set of relationships shown in Figs. 8 and 9. Because OIB glasses are degassed in CO_2 to variable degrees, we estimate primary melt (undegassed) CO_2 for OIB glasses in the following way. First, using a new correlation between undegassed CO_2/Nb and $(La/Sm)_N$ in MORB and OIB (see equation in Fig. 9a and discussion in Supplementary Information section S1.8), together with the measured $(La/Sm)_N$ available in

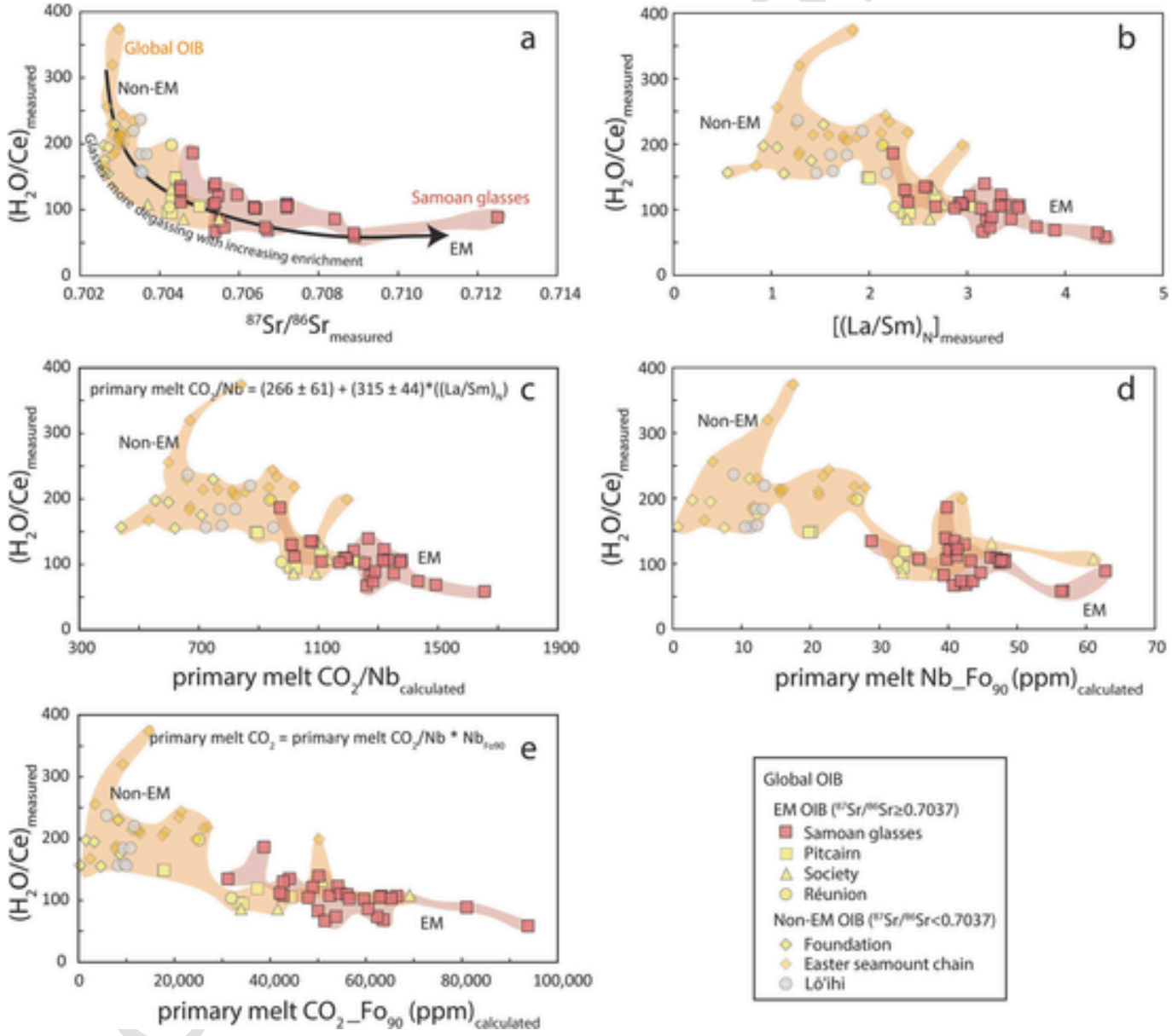

Fig. 8. Samoan pillow glasses compared to a global dataset of submarine OIB glasses, which show a trend of decreasing H_2O/Ce with increasing $^{87}Sr/^{86}Sr$. The exact same OIB dataset is shown in all panels: only OIB with $^{87}Sr/^{86}Sr$ data (to establish the level of source enrichment) and MgO > 4.5 wt% (to minimize the impact of fractional crystallization) are shown. (a) H_2O/Ce versus $^{87}Sr/^{86}Sr$. (b) H_2O/Ce versus $(La/Sm)_N$. (c) H_2O/Ce versus primary melt CO_2/Nb, where CO_2/Nb is calculated from the measured $(La/Sm)_N$ ratios using a linear fit between CO_2/Nb and $(La/Sm)_N$ (see equation shown in panel c) that is produced from a global data compilation of least degassed glasses and melt inclusions from OIB and MORB in Fig. 9. (d) H_2O/Ce versus calculated primary melt Nb for each sample, where primary melt Nb is calculated by olivine addition (or subtraction) from melt—following methods in text—until the melt is in equilibrium with Fo_{90} olivine. (e) H_2O/Ce versus calculated primary melt CO_2, where the CO_2 is calculated for each lava by multiplying the calculated CO_2/Nb (panel c) with the calculated primary melt Nb (panel d) (see equation in panel e). The same sources of data and data treatment as that described in the Fig. 7 caption are used here. The calculated primary melt CO_2/Nb and CO_2-Fo_{90} (ppm) values for the global OIB data set presented here are given in Table S11. Only samples with CO_2-H_2O saturation pressures ≥0.1 kbar are shown (just one Samoan glass with $^{87}Sr/^{86}Sr$ data has a saturation pressure <0.1 kbar, sample AVON3-68-03 Rpt, so its removal does not significantly impact the dataset).

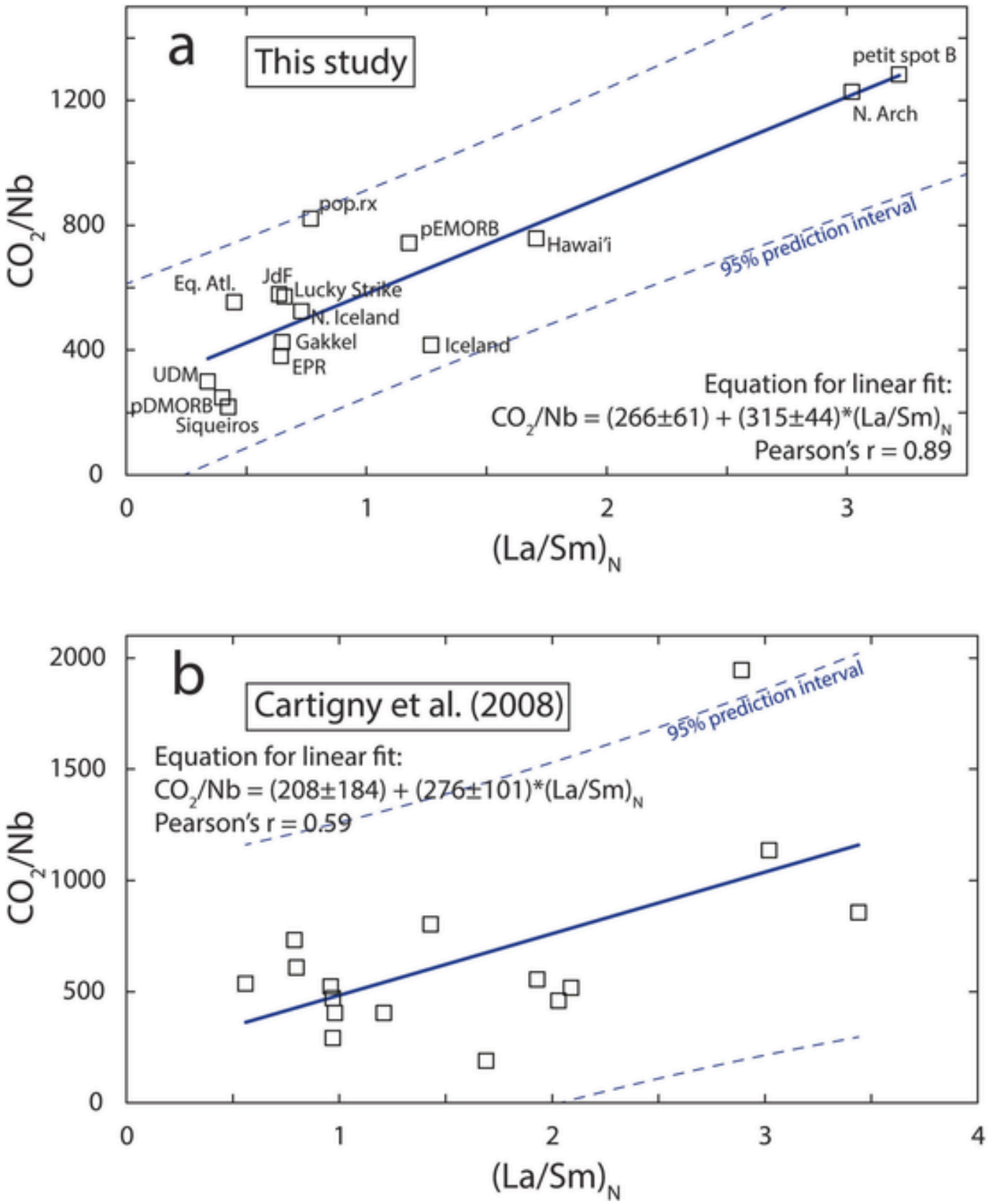

Fig. 9. (a) Linear fit (blue line) of global MORB and OIB glasses and melt inclusions with respect to CO_2/Nb and $(La/Sm)_N$. Data compilation is the same as what is presented in Fig. 1 of Hirschmann (2018). The values for CO_2/Nb and $(La/Sm)_N$ in panel (a) are given in Table S10. The blue dashed lines represent the 95% prediction interval. The 95% confidence interval of the linear fit is given with the equation of the linear fit. The linear relationship calculated in panel a is used to estimate

the suite of OIB glasses examined here, we can calculate the primary

Fig. 9.—*continued*
the CO_2/Nb values for glasses and melt inclusions in Fig. 8. (b) Linear fit (blue line) to the Mid-Atlantic Ridge CO_2/Nb versus $(La/Sm)_N$ data from Cartigny et al. (2008). The blue dashed lines are the 95% prediction bands for the linear fit using Cartigny et al. (2008) data. Sources of data for panel a: L. Strike (Lucky Strike): Wanless et al. (2015); JdF, EPR (Juan de Fuca, East Pacific Rise): Wanless and Shaw (2012); Gakkel: Wanless et al. (2014); Siqueiros: Saal et al. (2002); pEMORB and pDMORB (Pacific enriched and depleted MORB): Shimizu et al. (2016); UDM (ultra-depleted MORB): Michael and Graham (2015); pop.rx (North Atlantic popping rocks): Cartigny et al. (2008); Eq. Atl. (Equatorial Atlantic): Le Voyer et al. (2017); Iceland: Hartley et al. (2014); N. Iceland (Borgarhraun): Hauri et al. (2018); N. Arch (North Arch, Hawai'i): Dixon et al. (1997), Frey et al. (2000); Hawai'i (Kīlauea): Anderson and Poland (2017); Petit Spot B (Western Pacific seamounts): Machida et al. (2015). (For interpretation of the references to color in this figure legend, the reader is referred to the web version of this article.)

melt CO_2/Nb in the OIB glasses (Fig. 8c). (It is worth noting that the correlation between CO_2/Nb and $(La/Sm)_N$ in Fig. 9a is similar to a relationship previously suggested for MORB by Cartigny et al. (2008) (Fig. 9b).) We then calculate the primary melt Nb concentrations for each of the OIB glasses by correcting for olivine addition or subtraction so the melts are in equilibrium with mantle (Fo_{90}) olivine (Fig. 8d). By multiplying calculated primary melt CO_2/Nb (Fig. 8c) by the calculated primary melt Nb concentrations (Fig. 8d), we obtain primary melt CO_2 concentrations for the OIB glasses (Fig. 8e). These calculations suggest that the most extreme EM OIB glasses (which have the lowest H_2O/Ce) —all from the Samoa, Societies, and Pitcairn hotspots—tend to have the highest primary melt CO_2 (Fig. 8e), with CO_2 concentrations commonly as high as 5 to 6 wt% in Samoa and Societies lavas (and higher than 80,000 ppm CO_2 in two Samoan lavas). These high OIB primary melt CO_2 concentrations calculated with our new model are in broad agreement with CO_2 concentrations calculated using the petrologic model of Sun and Dasgupta (2020) (see supplementary Fig. S9 for direct comparison).

Based on these calculations, Samoan primary melts inferred from the pillow rim glass data have CO_2 concentrations between ~28,000 ppm and ~94,000 ppm, with most values clustering near ~60,000 ppm CO_2 (Fig. 8e). With few exceptions, the non-EM OIB (which have the highest erupted H_2O/Ce)—Lō'ihi, Easter, and Foundation—have lower calculated primary melt CO_2 than the EM OIB—Samoa, Societies, Pitcairn, and Réunion (Fig. 8e). This is consistent with prior suggestions that geochemically enriched mantle domains with higher $^{87}Sr/^{86}Sr$ generate primary melts with higher CO_2 than geochemically depleted mantle domains (Burnard et al., 2014; Cartigny et al., 2008; Le Voyer et al., 2019). Like Burnard et al. (2014), we argue that melts with higher initial CO_2—characteristic of EM melts (Fig. 8e)—undergo greater degrees of degassing than melts with lower initial CO_2. We then show that, everything else being the same, higher initial CO_2 melts experience greater degassing of H_2O (and thus have lower erupted H_2O/Ce) than melts with lower initial CO_2 (Fig. 8).

In order to demonstrate this quantitatively, we use the calculated primary melt CO_2 of the OIB glasses in Fig. 8e, as well as estimated primary melt H_2O (see below), as inputs to a closed-system degassing model. We then show that the CO_2-rich (60,000 ppm) model primary melt degasses by closed-system degassing to have H_2O concentration and H_2O/Ce similar to values measured in Samoan EM pillow glasses. To test our hypothesis that high primary melt CO_2 concentrations results in more degassing of H_2O, and thus, lower H_2O/Ce in the final erupted and degassed melt, we examine how H_2O and CO_2 concentrations change with decreasing pressure starting with two hypothetical primary melts that are identical in all respects except for the initial CO_2 concentrations: the two melt endmembers are given the same starting H_2O (2 wt%), H_2O/Ce (200), and major and trace element chemistry (see compositions in Table S9). The first model melt is assigned a higher CO_2 concentration of 60,000 ppm, meant to approximate the elevated CO_2 concentration of EM glasses in Fig. 8e (see previous paragraph), and comes from our new model for calculating CO_2 in OIB primary melts (Fig. 8c, 9a) for which calculated Samoan primary melt CO_2 concentrations tend to cluster near 60,000 ppm CO_2. The second model melt is assigned an initial CO_2 concentration of 5000 ppm, and is meant to approximate the CO_2 concentration of the non-EM glasses from Foundation, Easter, and Lō'ihi in Fig. 8e. In order to illustrate the impact of H_2O loss during degassing as a function of initial primary melt CO_2 concentration, we model the closed-system degassing paths of the two melts using rhyolite-MELTS. Degassing of the high CO_2 (60,000 ppm) melt starts at 26 kbar (i.e., where CO_2 first saturates; see dark green line in Fig. 10), which is higher than the 4 kbar pressure where the lower CO_2 melt saturates (see light green line in Fig. 10). After both the high- and low-CO_2 melts degas to the same low eruptive pressure (Fig. 10) —0.5 kbar, meant to represent pressure for eruption on the seafloor at ~5000 mbsl—the high CO_2 melt has a significantly lower H_2O concentration and lower H_2O/Ce (~0.94 wt% and 94, respectively) compared to the low CO_2 melt (~1.56 wt% wt% and 156, respectively), even though both melts started with the same H_2O (2 wt%) and H_2O/Ce (200). In summary, a melt with initial CO_2 of 60,000 ppm degases nearly 53% of its H_2O (and 99.4% of its CO_2) during ascent to 0.5 kbar, but the melt with 5000 ppm initial CO_2 degases just 22% of its H_2O (and 96.8% of its CO_2) during ascent to 0.5 kbar. Thus, everything else being the same, high CO_2 melts degas more H_2O and have lower H_2O/Ce than low CO_2 melts.

The simple degassing model in Fig. 10 helps explain the observation that EM pillow glasses erupted on the seafloor have lower H_2O/Ce compared to non-EM pillow glasses: EM primary melts, which are associated with higher initial CO_2 (Fig. 8e), saturate in volatiles deeper in the crust/mantle and degas more CO_2 and H_2O prior to eruption than non-EM melts with lower primary melt CO_2. The Samoan melt inclusions in this study exhibit high H_2O/Ce, similar to non-EM melts, because CO_2 and H_2O degassing was arrested following melt inclusion entrapment in olivine at high pressures (0.870 to 5.13 kbar). Although the Samoan melt inclusions lost significant amounts of CO_2 prior to being entrapped by olivine, these melt inclusions still preserve higher H_2O/Ce than the erupted pillow glasses due to having degassed less CO_2 and, thus, less H_2O. However, we acknowledge that, prior to entrapment, even the melt inclusions may have already lost some H_2O due to concomitant loss of both H_2O and CO_2 during closed-system degassing. Nonetheless, melt inclusions preserve higher H_2O and H_2O/Ce than pillow glasses, and thus preserve values closer to the primary melts.

6.4. Comparison with prior models for the origin of low H_2O/Ce in EM lavas, and implications for a "damp" EM mantle

Previous studies have suggested that the negative correlation between H_2O/Ce and $^{87}Sr/^{86}Sr$ is the result of dehydration (H_2O depletion) in the EM source, which has low H_2O/Ce that gives rise to EM primary melts with low H_2O/Ce. In these models, the EM mantle source has low H_2O/Ce because subducted materials contributing to the EM mantle lose H_2O during subduction (Dixon et al., 2002) or via diffusion during residence in the mantle (Workman et al., 2006), or because the pyroxenite—which has low H_2O/Ce—contributes to the EM mantle (Bizimis and Peslier, 2015). However, if these models explained the origin of the low H_2O/Ce in high $^{87}Sr/^{86}Sr$ glasses from Samoa, then the Samoan melt inclusions with high $^{87}Sr/^{86}Sr$ should also exhibit lower H_2O/Ce, but this is not the case.

Thus, an important implication is that submarine glasses cannot be reliably used to estimate the H_2O/Ce content of OIB primary melts, particularly glasses for EM OIB that appear to experience greater degassing (owing to higher initial CO_2) than non-EM OIB. Our data show that, unlike Samoan submarine glasses, Samoan melt inclusions have similar

UNCORRECTED PROOF

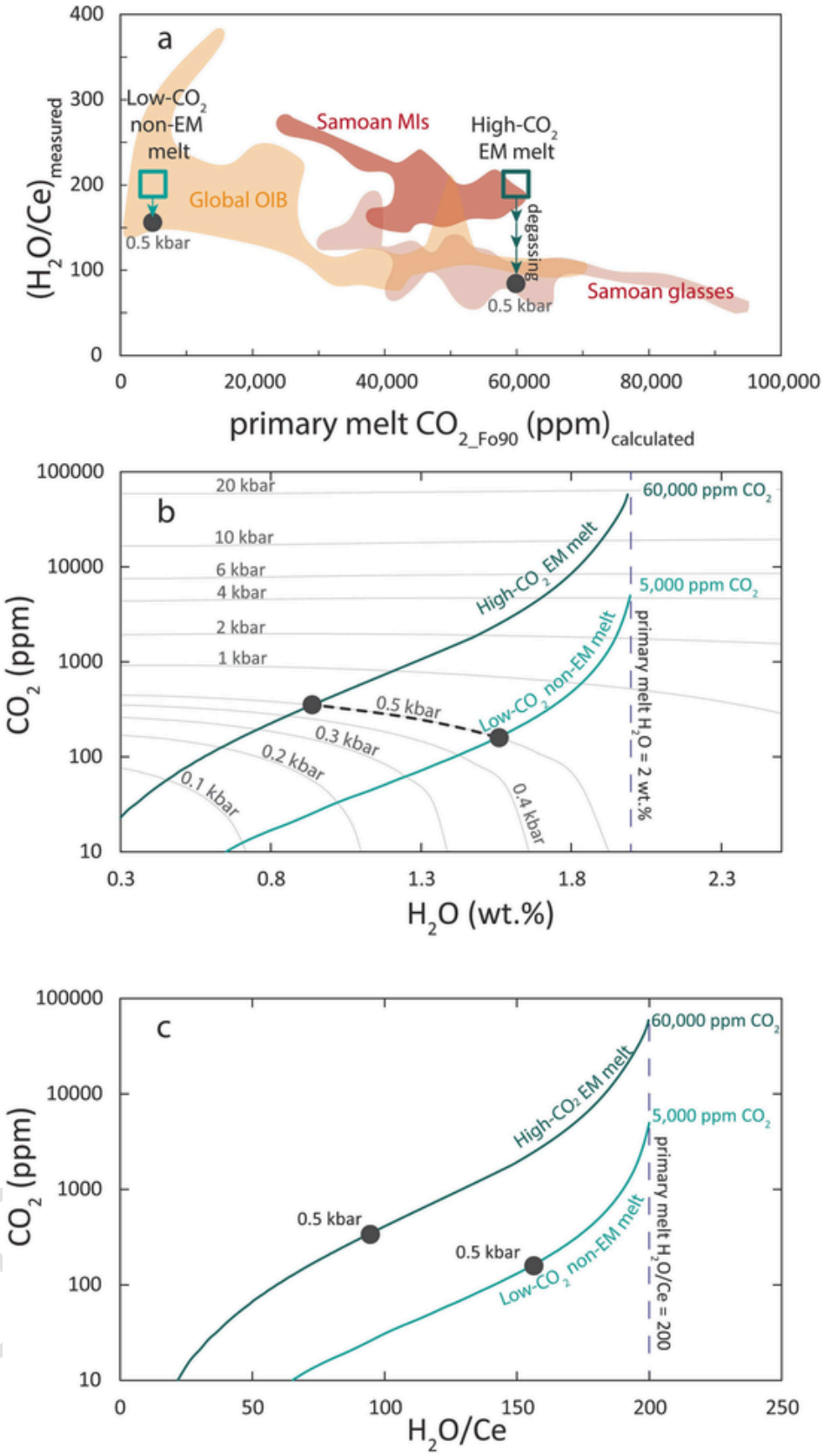

Fig. 10. Figure illustrating how submarine glasses from enriched mantle (EM) sources acquire low H_2O/Ce relative to glasses from non-EM sources. We test two melt compositions that are identical in every way (major and trace element compositions are identical and H_2O is 2 wt%) except for CO_2, where one melt starts with 60,000 ppm CO_2 (meant to represent an EM melt) and the other melt starts with 5000 ppm CO_2 (meant to represent the non-EM melt). (a) H_2O/Ce versus

Fig. 10.—*continued*
primary melt CO_2, reproduced in cartoon form from Fig. 8e. The black circle indicates the H_2O/Ce value for melts at 0.5 kbar after degassing. (b) In a plot of CO_2 versus H_2O, modeled closed system degassing paths show the impact of varying initial CO_2 on a melt that has the same initial H_2O content of 2 wt%. While both melts start with the same initial H_2O, those with higher initial CO_2 degas more H_2O and have lower H_2O at a given isobar compared to a melt that has lower initial CO_2, demonstrating how higher initial CO_2 results in lower H_2O (and lower H_2O/Ce) in the erupted lavas. Degassing trends assume oxygen fugacity (QFM) and temperature (1200 °C) and are calculated in rhyolite-MELTS v1.2 using AVON3-78-1#3 major element melt inclusion composition. Bottom panel shows the same degassing paths as the upper panels but shows H_2O/Ce instead of H_2O. Calculation of H_2O/Ce along the degassing paths assumes 1) an initial H_2O/Ce value of 200 (similar to the average H_2O/Ce value of Samoan melt inclusions examined here) and 2) a constant melt Ce concentration (100 ppm) that is calculated using the initial H_2O/Ce ratio (i.e., 200) and the initial H_2O (2 wt%). Similar to the relationship between CO_2 and H_2O for high and low CO_2 melts, at a given isobar the melt with high initial CO_2 has significantly lower H_2O/Ce compared to the melt with lower initial CO_2. Isobars are calculated using MagmaSat for the average Malumalu melt inclusion composition at 1200 °C. We consider only the case of M = 0 to highlight the role of initial CO_2 and saturation pressure on the H_2O content of a glass, and non-zero M values would result in even more rapid H_2O loss.

H_2O/Ce (197 ± 58, 2SD, N = 15) that does not vary with $^{87}Sr/^{86}Sr$. In fact, the H_2O/Ce ratio (193 ± 19, 2SD, N = 4) for extreme Samoan EM2 ($^{87}Sr/^{86}Sr$ > 0.708) melt inclusions overlaps with H_2O/Ce suggested for depleted mantle domains that are sampled by non-EM OIB ($^{87}Sr/^{86}Sr$ < 0.7037; H_2O/Ce = 209 ± 92), average Pacific MORB (180 ± 20; Dixon et al., 2017), average depleted N. Atlantic MORB (230 ± 20; Dixon et al., 2017), and PREMA (*Pre*valent *Ma*ntle) Pacific and Atlantic OIB (215 ± 30 and 220 ± 30, respectively, where PREMA-type OIB do not bear EM or HIMU signatures; Dixon et al., 2017). Thus, the major implication of this work is that, instead of being "dry", the EM2 mantle sampled by Samoa is just as "damp" as non-EM reservoirs, but this can only be seen by examining deeply entrapped melt inclusions that preserve higher CO_2 and H_2O than submarine pillow glasses. Due to pronounced CO_2 and concomitant H_2O degassing that appears to impact enriched lavas more than depleted ones—owing to higher primary melt CO_2 in the former relative to the latter—future melt inclusion studies will be important for determining the initial H_2O/Ce in EM1 (Pitcairn) and other EM2 (Societies) lavas, where existing low H_2O/Ce values measured in high $^{87}Sr/^{86}Sr$ Pitcairn and Societies submarine glasses (Kendrick et al., 2014) may also be due to the same degassing mechanism that lowers H_2O/Ce in Samoan OIB. If so, H_2O/Ce in the mantle is not likely to be as variable as previously supposed, and much of the mantle sampled by MORB and OIB have very similar H_2O/Ce that is, on average, close to a value of 200, and not as low as values found in pillow glasses of EM lavas (down to 59 in Samoan pillow glasses, 86 in Societies glasses, and 95 in Pitcairn glasses). Thus, like the Pb/Ce ratio, which is similar in OIB and MORB globally (Hofmann et al., 1986), the H_2O/Ce ratio may also be similar in the sources of plume-derived lavas (Michael, 1995).

A second implication of "damp" H_2O/Ce in EM Samoan lavas is that, in spite of hosting subducted continental materials which have presumably lost H_2O by degassing at an ancient subduction zone (White and Hofmann, 1982; Farley et al., 1992; Jackson et al., 2007), Samoan EM2 melt (as sampled by EM melt inclusions) do not have lower H_2O/Ce than non-EM OIBs. This is a surprising result, and suggests that recycled continental materials may not play a large role in governing the H_2O budgets of mantle domains. This could be because the amount of recycled continental crust in the mantle sources of OIB is small, and thus has a diminished impact on the overall H_2O and H_2O/Ce of the mantle source. For example, Samoan lava AVON3-78-1 examined in this study, which has a strong EM2 signature ($^{87}Sr/^{86}Sr$ of 0.7089), is estimated to have only ~1% continental crust (Reinhard et al., 2018) that is added to a depleted plume component that constitutes the rest (99%) of the mantle source. In this model, the H_2O and Ce budgets of the EM2 mantle source is primarily controlled by the depleted plume component, even if the recycled continental crust component has low H_2O/Ce. In this way, both depleted mantle and EM OIB can have similar H_2O/Ce.

CRediT authorship contribution statement

O.E. Anderson: Conceptualization, Formal analysis, Investigation, Project administration, Visualization, Writing – original draft, Writing – review & editing, Methodology. **M.G. Jackson:** Conceptualization, Funding acquisition, Writing – review & editing, Project administration, Resources, Supervision. **A.S. Pamukçu:** Investigation, Supervision, Writing – review & editing. **E.F. Rose-Koga:** Investigation, Writing – review & editing. **V. Le Roux:** Resources, Writing – review & editing. **F. Klein:** Methodology, Resources, Writing – review & editing. **K.T. Koga:** Formal analysis, Methodology, Writing – review & editing. **G.A. Gaetani:** Resources, Supervision, Writing – review & editing. **A.A. Price:** Investigation, Supervision, Writing – review & editing.

Uncited references

Le Voyer et al., 2019
Ryan et al., 2009

Declaration of competing interest

The authors declare that they have no known competing financial interests or personal relationships that could have appeared to influence the work reported in this paper.

Data availability

The data is shared as a supplementary Excel spreadsheet.

Acknowledgements

We would like to thank an anonymous reviewer for their constructive comments that led to a stronger manuscript. MGJ gratefully acknowledges being wrong (and that John Lassiter was correct) in the debate about whether mantle source H_2O/Ce is preserved in deeply dredged (>1000 mbsl) submarine pillow glasses. OEA thanks Marc Hirschmann for a discussion about CO_2/Nb in oceanic lavas, Gareth Seward for his skillful assistance with UCSB's EPMA, Jean-Luc Devidal for assisting EFR-K with LA-ICP-MS analyses, and Brian Monteleone for his time and help with SIMS analyses. MGJ acknowledges NSF grants OCE-1736984, EAR-1900652, OCE-1912931, and OCE-1929095 that supported this work.

Appendix A. Supplementary data

Supplementary data to this article can be found online at https://doi.org/10.1016/j.chemgeo.2024.121979.

References

Anderson, A.T., 1974. Evidence for a picritic, volatile-rich magma beneath Mt. Shasta, California. J. Petrol. 15, 243–267. https://doi.org/10.1093/petrology/15.2.243.
Anderson, K.R., Poland, M.P., 2017. Abundant carbon in the mantle beneath Hawai'i. Nat. Geosci. 10 (9), 704–708. https://doi.org/10.1038/ngeo3007.
Anderson, O.E., Jackson, M.G., Rose-Koga, E.F., Marske, J.P., Peterson, M.E., Price, A.A., Byerly, B.L., Reinhard, A.A., 2021. Testing the recycled gabbro hypothesis for the origin of "ghost plagioclase" melt signatures using $^{87}Sr/^{86}Sr$ of individual olivine-hosted melt inclusions from Hawai'i. Geochem. Geophys. Geosyst. 22 (4). https://doi.org/10.1029/2020GC009260.
Asimow, P.D., Langmuir, A.C., 2003. The importance of water to oceanic mantle melting

CORRECTED PROOF

regimes. Nature 421 (6925), 815–820. https://doi.org/10.1038/nature01429.
Aster, E.M., Wallace, P.J., Moore, L.R., Watkins, J., Gazel, E., Bodnar, R.J., 2016. Reconstructing CO_2 concentrations in basaltic melt inclusions using Raman analysis of vapor bubbles. J. Volcanol. Geotherm. Res. 323, 148–162. https://doi.org/10.1016/j.jvolgeores.2016.04.028.
Bizimis, M., Peslier, A.H., 2015. Water in Hawaiian garnet pyroxenites: Implications for water heterogeneity in the mantle. Chem. Geol. 397, 61–75. https://doi.org/10.1016/j.chemgeo.2015.01.008.
Blundy, J., Cashman, K.V., Rust, A., Witham, F., 2010. A case for CO_2-rich arc magmas. Earth Planet. Sci. Lett. 290 (3–4), 289–301. https://doi.org/10.1016/j.epsl.2009.12.013.
Bryan, W.B., Moore, J.G., 1977. Compositional variations of young basalts in the Mid-Atlantic Ridge rift valley near 36° 49′. Geological Society of America Bulletin 88, 556–570.
Bucholz, C.E., Gaetani, G.A., Behn, M.D., Shimizu, N., 2013. Post-entrapment modification of volatiles and oxygen fugacity in olivine-hosted melt inclusions. Earth Planet. Sci. Lett. 374, 145–155. https://doi.org/10.1016/j.epsl.2013.05.033.
Burnard, P., Reisberg, L., Colin, A., 2014. An observed link between lithophile compositions and degassing of volatiles (He, Ar, CO_2) in MORBs with implications for Re volatility and the mantle C/Nb ratio. Earth Planet. Sci. Lett. 395, 159–167. https://doi.org/10.1016/j.epsl.2014.03.045.
Cabral, R.A., Jackson, M.G., Koga, K.T., Rose-Koga, E.F., Hauri, E.H., Whitehouse, M.J., Price, A.A., Day, J.M., Shimizu, N., Kelley, K.A., 2014. Volatile cycling of H_2O, CO_2, F, and Cl in the HIMU mantle: a new window provided by melt inclusions from oceanic hot spot lavas at Mangaia, Cook Islands. Geochem. Geophys. Geosyst. 15 (11), 4445–4467. https://doi.org/10.1002/2014GC005473.
Cartigny, P., Pineau, F., Aubaud, C., Javoy, M., 2008. Towards a consistent mantle carbon flux estimate: Insights from volatile systematics (H_2O/Ce, δD, CO_2/Nb) in the North Atlantic mantle (14 N and 34 N). Earth Planet. Sci. Lett. 265 (3–4), 672–685. https://doi.org/10.1016/j.epsl.2007.11.011.
Danyushevsky, L.V., Della-Pasqua, F.N., Sokolov, S., 2000. Re-equilibration of melt inclusions trapped by magnesian olivine phenocrysts from subduction-related magmas: petrological implications. Contrib. Mineral. Petrol. 138 (1), 68–83. https://doi.org/10.1007/PL00007664.
Devey, C.W., Albarede, F., Cheminée, J.L., Michard, A., Mühe, R., Stoffers, P., 1990. Active submarine volcanism on the Society hotspot swell (West Pacific): a geochemical study. J. Geophys. Res. Solid Earth 95 (B4), 5049–5066. https://doi.org/10.1029/JB095iB04p05049.
DeVitre, C.L., Allison, C.M., Gazel, E., 2021. A high-precision CO_2 densimeter for Raman spectroscopy using a fluid density calibration apparatus. Chem. Geol. 584, 120522. https://doi.org/10.1016/j.chemgeo.2021.120522.
Dixon, J.E., Clague, D.A., 2001. Volatiles in basaltic glasses from Loihi Seamount, Hawaii: evidence for a relatively dry plume component. J. Petrol. 42 (3), 627–654. https://doi.org/10.1093/petrology/42.3.627.
Dixon, J.E., Clague, D.A., Wallace, P., Poreda, R., 1997. Volatiles in alkalic basalts form the North Arch Volcanic Field, Hawaii: extensive degassing of deep submarine-erupted alkalic series lavas. J. Petrol. 38 (7), 911–939. https://doi.org/10.1093/petroj/38.7.911.
Dixon, J.E., Leist, L., Langmuir, C., Schilling, J.G., 2002. Recycled dehydrated lithosphere observed in plume-influenced mid-ocean-ridge basalt. Nature 420 (6914), 385–389. https://doi.org/10.1038/nature01215.
Dixon, J.E., Bindeman, I.N., Kingsley, R.H., Simons, K.K., Le Roux, P.J., Hajewski, T.R., Swart, P., Langmuir, C.H., Ryan, J.G., Walowski, K.J., Wada, I., 2017. Light stable isotopic compositions of enriched mantle sources: Resolving the dehydration paradox. Geochem. Geophys. Geosyst. 18 (11), 3801–3839. https://doi.org/10.1002/2016GC006743.
Farley, K.A., Natland, J.H., Craig, H., 1992. Binary mixing of enriched and undegassed (primitive?) mantle components (He, Sr, Nd, Pb) in Samoan lavas. Earth Planet. Sci. Lett. 111 (1), 183–199. https://doi.org/10.1016/0012-821X(92)90178-X.
Ford, C.E., Russell, D.G., Craven, J.A., Fisk, M.R., 1983. Olivine-liquid equilibria: temperature, pressure and composition dependence of the crystal/liquid cation partition coefficients for Mg, Fe^{2+}, Ca and Mn. J. Petrol. 24 (3), 256–266. https://doi.org/10.1093/petrology/24.3.256.
Fortin, M.A., Riddle, J., Desjardins-Langlais, Y., Baker, D.R., 2015. The effect of water on the sulfur concentration at sulfide saturation (SCSS) in natural melts. Geochim. Cosmochim. Acta 160, 100–116. https://doi.org/10.1016/j.gca.2015.03.022.
Fretzdorff, S., Haase, K.M., 2002. Geochemistry and petrology of lavas from the submarine flanks of Réunion Island (western Indian Ocean): implications for magma genesis and the mantle source. Mineral. Petrol. 75, 153–184. https://doi.org/10.1007/s007100200022.
Frey, F.A., Clague, D., Mahoney, J.J., Sinton, J.M., 2000. Volcanism at the edge of the Hawaiian plume: petrogenesis of submarine alkalic lavas from the North Arch volcanic field. J. Petrol. 41 (5), 667–691. https://doi.org/10.1093/petrology/41.5.667.
Frezzotti, M.L., 2001. Silicate-melt inclusions in magmatic rocks: applications to petrology. Lithos 55 (1–4), 273–299. https://doi.org/10.1016/S0024-4937(00)00048-7.
Gaetani, G.A., Grove, T.L., 1998. The influence of water on melting of mantle peridotite. Contrib. Mineral. Petrol. 131, 323–346. https://doi.org/10.1007/s004100050396.
Gaetani, G.A., O'Leary, J.A., Shimizu, N., Bucholz, C.E., Newville, M., 2012. Rapid reequilibration of H_2O and oxygen fugacity in olivine-hosted melt inclusions. Geology 40 (10), 915–918. https://doi.org/10.1130/G32992.1.
Gale, A., Dalton, C.A., Langmuir, C.H., Su, Y., Schilling, J.G., 2013. The mean composition of ocean ridge basalts. Geochemistry, Geophysics, Geosystems 14 (3), 489–518. https://doi.org/10.1029/2012GC004334.
Gerlach, T.M., Taylor, B.E., 1990. Carbon isotope constraints on degassing of carbon dioxide from Kilauea Volcano. Geochim. Cosmochim. Acta 54 (7), 2051–2058. https://doi.org/10.1016/0016-7037(90)90270-U.
Ghiorso, M.S., Gualda, G.A., 2015. An H_2O–CO_2 mixed fluid saturation model compatible with rhyolite-MELTS. Contrib. Mineral. Petrol. 169, 1–30. https://doi.org/10.1007/s00410-015-1141-8.
Graham, D.W., Michael, P.J., 2021. Predominantly recycled carbon in Earth's upper mantle revealed by He-CO_2-Ba systematics in ultradepleted ocean ridge basalts. Earth Planet. Sci. Lett. 554, 116646. https://doi.org/10.1016/j.epsl.2020.116646.
Gualda, G.A.R., Ghiorso, M.S., Lemons, R.V., Carley, T.L., 2012. Rhyolite-MELTS: a modified calibration of MELTS optimized for silica-rich, fluid-bearing magmatic systems. J. Petrol. 53, 875–890. https://doi.org/10.1093/petrology/egr080.
Hanyu, T., Yamamoto, J., Kimoto, K., Shimizu, K., Ushikubo, T., 2020. Determination of total CO_2 in melt inclusions with shrinkage bubbles. Chem. Geol. 557, 119855. https://doi.org/10.1016/j.chemgeo.2020.119855.
Hart, S.R., 1988. Heterogeneous mantle domains: signatures, genesis and mixing chronologies. Earth Planet. Sci. Lett. 90 (3), 273–296. https://doi.org/10.1016/0012-821X(88)90131-8.
Hart, S.R., Gerlach, D.C., White, W.M., 1986. A possible new Sr-Nd-Pb mantle array and consequences for mantle mixing. Geochim. Cosmochim. Acta 50 (7), 1551–1557. https://doi.org/10.1016/0016-7037(86)90329-7.
Hartley, M.E., Maclennan, J., Edmonds, M., Thordarson, T., 2014. Reconstructing the deep CO_2 degassing behaviour of large basaltic fissure eruptions. Earth Planet. Sci. Lett. 393, 120–131. https://doi.org/10.1016/j.epsl.2014.02.031.
Hartley, M.E., Neave, D.A., Maclennan, J., Edmonds, M., Thordarson, T., 2015. Diffusive over-hydration of olivine-hosted melt inclusions. Earth Planet. Sci. Lett. 425, 168–178. https://doi.org/10.1016/j.epsl.2015.06.008.
Hauri, E.H., 1996. Major-element variability in the Hawaiian mantle plume. Nature 382 (6590), 415–419. https://doi.org/10.1038/382415a0.
Hauri, E., 2002. SIMS analysis of volatiles in silicate glasses, 2: isotopes and abundances in Hawaiian melt inclusions. Chem. Geol. 183 (1–4), 115–141. https://doi.org/10.1016/S0009-2541(01)00374-6.
Hauri, E.H., Hart, S.R., 1993. ReOs isotope systematics of HIMU and EMII oceanic island basalts from the South Pacific Ocean. Earth Planet. Sci. Lett. 114 (2–3), 353–371. https://doi.org/10.1016/0012-821X(93)90036-9.
Hauri, E.H., Maclennan, J., McKenzie, D., Gronvold, K., Oskarsson, N., Shimizu, N., 2018. CO_2 content beneath northern Iceland and the variability of mantle carbon. Geology 46 (1), 55–58. https://doi.org/10.1130/G39413.1.
Hirschmann, M.M., 2006. Water, melting, and the deep Earth H_2O cycle. Annu. Rev. Earth Planet. Sci. 34, 629–653. https://doi.org/10.1146/annurev.earth.34.031405.125211.
Hirschmann, M.M., 2018. Comparative deep Earth volatile cycles: the case for C recycling from exosphere/mantle fractionation of major (H_2O, C, N) volatiles and from H_2O/Ce, CO_2/Ba, and CO_2/Nb exosphere ratios. Earth Planet. Sci. Lett. 502, 262–273. https://doi.org/10.1016/j.epsl.2018.08.023.
Hirth, G., Kohlstedf, D., 2003. Rheology of the upper mantle and the mantle wedge: a view from the experimentalists. Geophys. Monograph-Am. Geophys. Union 138, 83–106. https://doi.org/10.1029/138GM06.
Hirth, G., Kohlstedt, D.L., 1996. Water in the oceanic upper mantle: implications for rheology, melt extraction and the evolution of the lithosphere. Earth Planet. Sci. Lett. 144 (1–2), 93–108. https://doi.org/10.1016/0012-821X(96)00154-9.
Hofmann, A.W., White, W.M., 1982. Mantle plumes from ancient oceanic crust. Earth Planet. Sci. Lett. 57 (2), 421–436. https://doi.org/10.1016/0012-821X(82)90161-3.
Hofmann, A.W., Jochum, K.P., Seufert, M., White, W.M., 1986. Nb and Pb in oceanic basalts: new constraints on mantle evolution. Earth Planet. Sci. Lett. 79 (1–2), 33–45. https://doi.org/10.1016/0012-821X(86)90038-5.
Iacovino, K., Matthews, S., Wieser, P.E., Moore, G.M., Bégué, F., 2021. VESIcal Part I: an open-source thermodynamic model engine for mixed volatile (H_2O-CO_2) solubility in silicate melts. Earth Space Sci. 8 (11), e2020EA001584. https://doi.org/10.1029/2020EA001584.
Jackson, M.G., Hart, S.R., 2006. Strontium isotopes in melt inclusions from Samoan basalts: Implications for heterogeneity in the Samoan plume. Earth Planet. Sci. Lett. 245 (1–2), 260–277. https://doi.org/10.1016/j.epsl.2006.02.040.
Jackson, M.G., Macdonald, F.A., 2022. Hemispheric geochemical dichotomy of the mantle is a legacy of austral supercontinent assembly and onset of deep continental crust subduction. AGU Adv. 3 (6), e2022AV000664. https://doi.org/10.1029/2022AV000664.
Jackson, M.G., Kurz, M.D., Hart, S.R., Workman, R.K., 2007. New Samoan lavas from Ofu Island reveal a hemispherically heterogeneous high $^3He/^4He$ mantle. Earth Planet. Sci. Lett. 264 (3–4), 360–374. https://doi.org/10.1016/j.epsl.2007.09.023.
Jackson, M.G., Hart, S.R., Konter, J.G., Kurz, M.D., Blusztajn, J., Farley, K.A., 2014. Helium and lead isotopes reveal the geochemical geometry of the Samoan plume. Nature 514 (7522), 355–358. https://doi.org/10.1038/nature13794.
Jackson, M.G., Koga, K.T., Price, A., Konter, J.G., Koppers, A.A., Finlayson, V.A., Konrad, K., Hauri, E.H., Kylander-Clark, A., Kelley, K.A., Kendrick, M.A., 2015. Deeply dredged submarine HIMU glasses from the Tuvalu Islands, Polynesia: Implications for volatile budgets of recycled oceanic crust. Geochem. Geophys. Geosyst. 16 (9), 3210–3234. https://doi.org/10.1002/2015GC005966.
Kendrick, M.A., Arculus, R., Burnard, P., Honda, M., 2013. Quantifying brine assimilation by submarine magmas: examples from the Galápagos Spreading Centre and Lau Basin. Geochim. Cosmochim. Acta 123, 150–165. https://doi.org/10.1016/j.gca.2013.09.012.
Kendrick, M.A., Jackson, M.G., Kent, A.J., Hauri, E.H., Wallace, P.J., Woodhead, J., 2014. Contrasting behaviours of CO_2, S, H_2O and halogens (F, Cl, Br, and I) in enriched-mantle melts from Pitcairn and Society seamounts. Chem. Geol. 370, 69–81. https://doi.org/10.1016/j.chemgeo.2014.01.019.
Kendrick, M.A., Jackson, M.G., Hauri, E.H., Phillips, D., 2015. The halogen (F, Cl, Br, I)

UNCORRECTED PROOF

and H_2O systematics of Samoan lavas: Assimilated-seawater, EM2 and high-$^3He/^4He$ components. Earth Planet. Sci. Lett. 410, 197–209. https://doi.org/10.1016/j.epsl.2014.11.026.
Kendrick, M.A., Hémond, C., Kamenetsky, V.S., Danyushevsky, L., Devey, C.W., Rodemann, T., Jackson, M.G., Perfit, M.R., 2017. Seawater cycled throughout Earth's mantle in partially serpentinized lithosphere. Nat. Geosci. 10 (3), 222–228. https://doi.org/10.1038/ngeo2902.
Kent, A.J.R., Clague, D.A., Honda, M., Stolper, E.M., Hutcheon, I.D., Norman, M.D., 1999a. Widespread assimilation of a seawater-derived component at Loihi Seamount, Hawaii. Geochim. Cosmochim. Acta 63 (18), 2749–2761. https://doi.org/10.1016/S0016-7037(99)00215-X.
Kent, A.J.R., Norman, M.D., Hutcheon, I.D., Stolper, E.M., 1999b. Assimilation of seawater-derived components in an oceanic volcano: evidence from matrix glasses and glass inclusions from Loihi seamount, Hawaii. Chem. Geol. 156 (1–4), 299–319. https://doi.org/10.1016/S0009-2541(98)00188-0.
Kent, A.J.R., Peate, D.W., Newman, S., Stolper, E.M., Pearce, J.A., 2002. Chlorine in submarine glasses from the Lau Basin: seawater contamination and constraints on the composition of slab-derived fluids. Earth Planet. Sci. Lett. 202 (2), 361–377. https://doi.org/10.1016/S0012-821X(02)00786-0.
Koleszar, A.M., Saal, A.E., Hauri, E.H., Nagle, A.N., Liang, Y., Kurz, M.D., 2009. The volatile contents of the Galapagos plume; evidence for H_2O and F open system behavior in melt inclusions. Earth Planet. Sci. Lett. 287 (3–4), 442–452. https://doi.org/10.1016/j.epsl.2009.08.029.
Kumamoto, K.M., Warren, J.M., Hauri, E.H., 2017. New SIMS reference materials for measuring water in upper mantle minerals. American Mineralogist 102, 537–547. https://doi.org/10.2138/am-2017-5863CCBYNCND.
Labidi, J., Cartigny, P., Jackson, M.G., 2015. Multiple sulfur isotope composition of oxidized Samoan melts and the implications of a sulfur isotope 'mantle array' in chemical geodynamics. Earth Planet. Sci. Lett. 417, 28–39. https://doi.org/10.1016/j.epsl.2015.02.004.
Lassiter, J.C., Hauri, E.H., Nikogosian, I.K., Barsczus, H.G., 2002. Chlorine–potassium variations in melt inclusions from Raivavae and Rapa, Austral Islands: constraints on chlorine recycling in the mantle and evidence for brine-induced melting of oceanic crust. Earth Planet. Sci. Lett. 202 (3–4), 525–540. https://doi.org/10.1016/S0012-821X(02)00826-9.
Le Roux, P.J., Shirey, S.B., Hauri, E.H., Perfit, M.R., Bender, J.F., 2006. The effects of variable sources, processes and contaminants on the composition of northern EPR MORB (8–10°N and 12–14°N): evidence from volatiles (H_2O, CO_2, S) and halogens (F, Cl). Earth Planet. Sci. Lett. 251 (3–4), 209–231. https://doi.org/10.1016/j.epsl.2006.09.012.
Le Voyer, M., Kelley, K.A., Cottrell, E., Hauri, E.H., 2017. Heterogeneity in mantle carbon content from CO_2-undersaturated basalts. Nat. Commun. 8 (1), 14062. https://doi.org/10.1038/ncomms14062.
Le Voyer, M., Hauri, E.H., Cottrell, E., Kelley, K.A., Salters, V.J., Langmuir, C.H., Hilton, D.R., Barry, P.H., Füri, E., 2019. Carbon fluxes and primary magma CO_2 contents along the global mid-ocean ridge system. Geochem. Geophys. Geosyst. 20 (3), 1387–1424. https://doi.org/10.1029/2018GC007630.
Loewen, M.W., Graham, D.W., Bindeman, I.N., Lupton, J.E., Garcia, M.O., 2019. Hydrogen isotopes in high $^3He/^4He$ submarine basalts: Primordial vs. recycled water and the veil of mantle enrichment. Earth Planet. Sci. Lett. 508, 62–73. https://doi.org/10.1016/j.epsl.2018.12.012.
Machida, S., Hirano, N., Sumino, H., Hirata, T., Yoneda, S., Kato, Y., 2015. Petit-spot geology reveals melts in upper-most asthenosphere dragged by lithosphere. Earth Planet. Sci. Lett. 426, 267–279. https://doi.org/10.1016/j.epsl.2015.06.018.
Matthews, S., Shorttle, O., Rudge, J.F., Maclennan, J., 2017. Constraining mantle carbon: CO_2-trace element systematics in basalts and the roles of magma mixing and degassing. Earth Planet. Sci. Lett. 480, 1–14. https://doi.org/10.1016/j.epsl.2017.09.047.
Matthews, S., Shorttle, O., Maclennan, J., Rudge, J.F., 2021. The global melt inclusion C/Ba array: Mantle variability, melting process, or degassing? Geochim. Cosmochim. Acta 293, 525–543. https://doi.org/10.1016/j.gca.2020.09.030.
McDonough, W.F., Sun, S.S., 1995. The composition of the Earth. Chem. Geol. 120, 223–253. https://doi.org/10.1016/0009-2541(94)00140-4.
Métrich, N., Zanon, V., Créon, L., Hildenbrand, A., Moreira, M., Marques, F.O., 2014. Is the 'Azores hotspot'a wetspot? Insights from the geochemistry of fluid and melt inclusions in olivine of Pico basalts. J. Petrol. 55 (2), 377–393. https://doi.org/10.1093/petrology/egt071.
Michael, P., 1995. Regionally distinctive sources of depleted MORB: evidence from trace elements and H_2O. Earth Planet. Sci. Lett. 131 (3–4), 301–320. https://doi.org/10.1016/0012-821X(95)00023-6.
Michael, P.J., Graham, D.W., 2015. The behavior and concentration of CO_2 in the suboceanic mantle: Inferences from undegassed ocean ridge and ocean island basalts. Lithos 236, 338–351. https://doi.org/10.1016/j.lithos.2015.08.020.
Miller, W.G., Maclennan, J., Shorttle, O., Gaetani, G.A., Le Roux, V., Klein, F., 2019. Estimating the carbon content of the deep mantle with Icelandic melt inclusions. Earth Planet. Sci. Lett. 523, 115699. https://doi.org/10.1016/j.epsl.2019.07.002.
Moore, L.R., Gazel, E., Tuohy, R., Lloyd, A.S., Esposito, R., Steele-MacInnis, M., Hauri, E.H., Wallace, P.J., Plank, T., Bodnar, R.J., 2015. Bubbles matter: an assessment of the contribution of vapor bubbles to melt inclusion volatile budgets. Am. Mineral. 100 (4), 806–823. https://doi.org/10.2138/am-2015-5036.
Portnyagin, M., Hoernle, K., Plechov, P., Mironov, N., Khubunaya, S., 2007. Constraints on mantle melting and composition and nature of slab components in volcanic arcs from volatiles (H_2O, S, Cl, F) and trace elements in melt inclusions from the Kamchatka Arc. Earth Planet. Sci. Lett. 255 (1–2), 53–69. https://doi.org/10.1016/j.epsl.2006.12.005.
Portnyagin, M., Almeev, R., Matveev, S., Holtz, F., 2008. Experimental evidence for rapid water exchange between melt inclusions in olivine and host magma. Earth Planet. Sci. Lett. 272 (3–4), 541–552. https://doi.org/10.1016/j.epsl.2008.05.020.
Reinhard, A.A., Jackson, M.G., Koornneef, J.M., Rose-Koga, E.F., Blusztajn, J., Konter, J.G., Koga, K.T., Wallace, P.J., Harvey, J., 2018. Sr and Nd isotopic compositions of individual olivine-hosted melt inclusions from Hawai'i and Samoa: Implications for the origin of isotopic heterogeneity in melt inclusions from OIB lavas. Chem. Geol. 495, 36–49. https://doi.org/10.1016/j.chemgeo.2018.07.034.
Roeder, P.L., Emslie, R., 1970. Olivine-liquid equilibrium. Contrib. Mineral. Petrol. 29 (4), 275–289. https://doi.org/10.1007/BF00371276.
Rose-Koga, E.F., Koga, K.T., Schiano, P., Le Voyer, M., Shimizu, N., Whitehouse, M.J., Clocchiatti, R., 2012. Mantle source heterogeneity for South Tyrrhenian magmas revealed by Pb isotopes and halogen contents of olivine-hosted melt inclusions. Chem. Geol. 334, 266–279. https://doi.org/10.1016/j.chemgeo.2012.10.033.
Rose-Koga, E.F., Koga, K.T., Moreira, M., Vlastélic, I., Jackson, M.G., Whitehouse, M.J., Shimizu, N., Habib, N., 2017. Geochemical systematics of Pb isotopes, fluorine, and sulfur in melt inclusions from São Miguel, Azores. Chem. Geol. 458, 22–37. https://doi.org/10.1016/j.chemgeo.2017.03.024.
Rosenthal, A., Hauri, E.H., Hirschmann, M.M., 2015. Experimental determination of C, F, and H partitioning between mantle minerals and carbonated basalt, CO_2/Ba and CO_2/Nb systematics of partial melting, and the CO_2 contents of basaltic source regions. Earth Planet. Sci. Lett. 412, 77–87. https://doi.org/10.1016/j.epsl.2014.11.044.
Rowe, M.C., Lassiter, J.C., 2009. Chlorine enrichment in Central Rio Grande Rift basaltic melt inclusions: evidence for subduction modification of the lithospheric mantle. Geology 37 (5), 439–442. https://doi.org/10.1130/G25530A.1.
Rust, A.C., Cashman, K.V., Wallace, P.J., 2004. Magma degassing buffered by vapor flow through brecciated conduit margins. Geology 32 (4), 349–352. https://doi.org/10.1130/G20388.2.
Ryan, W.B.F., Carbotte, S.M., Coplan, J.O., O'Hara, S., Melkonian, A., Arko, R., Weissel, R.A., Ferrini, V., Goodwillie, A., Nitsche, F., Bonczkowski, J., Zemsky, R., 2009. Global multi-resolution topography synthesis. Geochem. Geophys. Geosyst. 10, Q03014. https://doi.org/10.1029/2008GC002332.
Saal, A.E., Hauri, E.H., Langmuir, C.H., Perfit, M.R., 2002. Vapour undersaturation in primitive mid-ocean-ridge basalt and the volatile content of Earth's upper mantle. Nature 419 (6906), 451–455. https://doi.org/10.1038/nature01073.
Shimizu, K., Saal, A.E., Myers, C.E., Nagle, A.N., Hauri, E.H., Forsyth, D.W., Kamenetsky, V.S., Niu, Y., 2016. Two-component mantle melting-mixing model for the generation of mid-ocean ridge basalts: Implications for the volatile content of the Pacific upper mantle. Geochim. Cosmochim. Acta 176, 44–80. https://doi.org/10.1016/j.gca.2015.10.033.
Shimizu, K., Saal, A.E., Hauri, E.H., Sinton, J.M., Janney, P.E., Geshi, N., Hékinian, R., 2023. High-C content and CO_2/Ba ratio of the Earth's enriched upper mantle. Geochim. Cosmochim. Acta. https://doi.org/10.1016/j.gca.2022.10.023.
Sims, K.W.W., Hart, S.R., Reagan, M.K., Blusztajn, J., Staudigel, H., Sohn, R.A., Layne, G.D., Ball, L.A., Andrews, J., 2008. 238U-230Th-226Ra-210Pb-210Po, 232Th-228Ra, and 235U-231Pa constraints on the ages and petrogenesis of Vailulu'u and Malumalu Lavas, Samoa. Geochem. Geophys. Geosyst. 9, Q04003. https://doi.org/10.1029/2007GC001651.
Smythe, D.J., Wood, B.J., Kiseeva, E.S., 2017. The S content of silicate melts at sulfide saturation: new experiments and a model incorporating the effects of sulfide composition. Am. Mineral. 102 (4), 795–803. https://doi.org/10.2138/am-2017-5800CCBY.
Staudigel, H., Zindler, A., Hart, S.R., Leslie, T., Chen, C.Y., Clague, D., 1984. The isotope systematics of a juvenile intraplate volcano: Pb, Nd, and Sr isotope ratios of basalts from Loihi Seamount, Hawaii. Earth Planet. Sci. Lett. 69 (1), 13–29. https://doi.org/10.1016/0012-821X(84)90071-2.
Sun, C., Dasgupta, R., 2020. Thermobarometry of CO_2-rich, silica-undersaturated melts constrains cratonic lithosphere thinning through time in areas of kimberlitic magmatism. Earth Planet. Sci. Lett. 550, 116549. https://doi.org/10.1016/j.epsl.2020.116549.
Taracsák, Z., Hartley, M.E., Burgess, R., Edmonds, M., Iddon, F., Longpré, M.A., 2019. High fluxes of deep volatiles from ocean island volcanoes: Insights from El Hierro, Canary Islands. Geochim. Cosmochim. Acta 258, 19–36. https://doi.org/10.1016/j.gca.2019.05.020.
Wallace, P.J., 2002. Volatiles in submarine basaltic glasses from the Northern Kerguelen Plateau (ODP Site 1140): Implications for source region compositions, magmatic processes, and plateau subsidence. J. Petrol. 43 (7), 1311–1326. https://doi.org/10.1093/petrology/43.7.1311.
Wanless, V.D., Shaw, A.M., 2012. Lower crustal crystallization and melt evolution at mid-ocean ridges. Nat. Geosci. 5 (9), 651–655. https://doi.org/10.1038/ngeo1552.
Wanless, V.D., Behn, M.D., Shaw, A.M., Plank, T., 2014. Variations in melting dynamics and mantle compositions along the Eastern Volcanic Zone of the Gakkel Ridge: insights from olivine-hosted melt inclusions. Contrib. Mineral. Petrol. 167, 1–22. https://doi.org/10.1007/s00410-014-1005-7.
Wanless, V.D., Shaw, A.M., Behn, M.D., Soule, S.A., Escartín, J., Hamelin, C., 2015. Magmatic plumbing at Lucky strike volcano based on olivine-hosted melt inclusion compositions. Geochem. Geophys. Geosyst. 16 (1), 126–147. https://doi.org/10.1002/2014GC005517.
White, W.M., Duncan, R.A., 1996. Geochemistry and geochronology of the Society Islands: New evidence for deep mantle recycling. Geophys. Monograph-Am. Geophys. Union 95, 183–206.
White, W.M., Hofmann, A.W., 1982. Sr and Nd isotope geochemistry of oceanic basalts and mantle evolution. Nature 296 (5860), 821–825. https://doi.org/10.1038/296821a0.
Wieser, P.E., Iacovino, K., Matthews, S., Moore, G., Allison, C.M., 2022. VESIcal: 2. A critical approach to volatile solubility modeling using an open-source Python3 engine. Earth Space Sci. 9 (2), e2021EA001932. https://doi.org/10.1029/

CORRECTED PROOF

2021EA001932.
Woodhead, J.D., Devey, C.W., 1993. Geochemistry of the Pitcairn seamounts, I: source character and temporal trends. Earth Planet. Sci. Lett. 116 (1–4), 81–99. https://doi.org/10.1016/0012-821X(93)90046-C.
Workman, R.K., Hart, S.R., Jackson, M., Regelous, M., Farley, K.A., Blusztajn, J., Kurz, M., Staudigel, H., 2004. Recycled metasomatized lithosphere as the origin of the Enriched Mantle II (EM2) end-member: evidence from the Samoan Volcanic Chain. Geochem. Geophys. Geosyst. 5 (4). https://doi.org/10.1029/2003GC000623.
Workman, R.K., Hauri, E., Hart, S.R., Wang, J., Blusztajn, J., 2006. Volatile and trace elements in basaltic glasses from Samoa: Implications for water distribution in the mantle. Earth Planet. Sci. Lett. 241 (3–4), 932–951. https://doi.org/10.1016/j.epsl.2005.10.028.
Zindler, A., Hart, S., 1986. Chemical geodynamics. Annu. Rev. Earth Planet. Sci. 14 (1), 493–571. https://doi.org/10.1146/annurev.ea.14.050186.002425.

CORRECTED PROOF